REVIEW ARTICLE

Check for updates

Catalysts for selective CO_2/CO electroreduction to C_{3+} compounds

Ngoc Huan Tran,[a] Moritz W. Schreiber[b] and Marc Fontecave [ID] *[a]

Electroreduction of carbon dioxide and carbon monoxide to organic compounds is considered a promising way for (i) exploring a source of carbon alternative to fossil carbon; (ii) storing electrical energy as stable chemical energy; and (iii) producing useful e-chemicals and e-fuels for the chemical industry. While it is generally considered that only Cu-based catalysts facilitate the formation of multicarbon compounds, which are mainly limited to ethylene and ethanol, recent studies have challenged this assumption. In this review, we provide exhaustive, structural and mechanistic analyses of the solid materials that have been reported as catalysts for electroreduction of CO_2 and CO to more complex molecules. This review elucidates that besides copper, metals such as nickel, iron and molybdenum have the potential to favor C–C coupling reactions to form important molecules in the chemical industry, such as propane, propanol, and butanol, along with offering substantial faradaic efficiencies. Thus, this review offers fresh perspectives on CO_2R and COR.

Broader context

The valorization of captured CO_2, as a source of carbon, *via* electroconversion into organic compounds useful for the chemical industry, such as hydrocarbons and alcohols, is one of the rare alternatives to the current petrochemistry. Because the reactions involve multiple electron- and proton-transfers, the development of this technology depends on the discovery of cheap, selective and efficient catalysts. However, research has mainly focused on Cu-based electrocatalysts that are appropriate for the production of methane, ethylene and ethanol, with less efforts devoted to catalysts for the more challenging electroconversion of CO_2 into C_{3+} molecules, containing three carbon atoms or more. This is unfortunate given that important feedstocks for the chemical industry belong to this category, such as propanol, propane, propylene, butane and butanol. This review provides an overview of the current state-of-the-art electrocatalysts used for CO_2 to C_{3+} product formation and provides directions for their further development.

Introduction

Because of anthropogenic CO_2 emissions and the resulting global warming, current energy policy trajectories aim at drastically and quickly reducing the combustion of fossil carbon sources, which currently represent more than 80% of the global energy consumption. Although this implies the massive electrification of transport, residential heating and industries *via* the development of low-carbon renewable (wind, solar and hydroelectric) and nuclear energy, some sectors will continue to rely on carbon-based compounds with high-energy densities, which are presently derived from fossil resources.[1,2] These sectors include functional organic chemical (solvents, polymers, and drugs) production, aviation and shipping. The

development of potential new sectors such as long-term energy storage and transport may also depend on these fuels. Accordingly, sustainable alternatives to fossil carbon, such as agricultural biomass and domestic and industrial waste can be used to produce (bio)methane, (bio)ethanol and (bio)diesel. However, the limited availability of these feedstocks allows only to replace a fraction of fossil resources that are currently used.[3]

CO_2 is a promising source of carbon as enough CO_2 is available in the atmosphere to fully replace the fossil-derived chemicals consumed by our society with e-fuels and e-chemicals.[4–7] CO_2 conversion has several advantages. Firstly, as it relies on CO_2 captured from point sources (power plants, cemeteries, steel factories, and digesters), with the possibility of direct capture from the air (DAC) in the future, the process is carbon neutral. Secondly, it provides a mechanism to convert renewable intermittent electricity into stable chemical energy (energy in chemical bonds) for long-term storage. Thirdly, it can convert CO_2, as a carbon source, into a variety of useful organic chemicals for the chemical industry and for

[a] Laboratoire de Chimie des Processus Biologiques, CNRS UMR 8229, Collège de France, Sorbonne Université, 11 Place Marcelin Berthelot, 75231 Cedex 05, Paris, France. E-mail: marc.fontecave@college-de-france.fr

[b] TotalEnergies OneTech Belgium, B-7181 Seneffe, Belgium

applications such as transport and heat production. However, currently, this approach is not industrially mature. The development of economically viable e-fuels and e-chemicals on a large scale will depend on successfully addressing the challenges encountered in the (i) massive production of cheap low-carbon electricity; (ii) cost-effective capture of massive amounts of CO_2; (iii) development of efficient electrolyzers (with high energy efficiency, high current density, high selectivity and long lifetime).

CO_2 valorization requires the initial conversion of electrical energy to chemical energy. The most mature pathways to convert CO_2 to organic molecules rely on H_2O electrolysis to H_2 and subsequent thermochemical reduction steps. Alternatively, CO_2 electroreduction (CO_2R) allows the synthesis of organic molecules in a single step. This has the potential to greatly increase the energy efficiency and reduce the capital expenditure required for this transformation compared with the electrolytic H_2 pathway.[8,9]

The CO_2R performance can be optimized *via* the appropriate development of electrolyzers and catalysts. Electrolyzers suffer from various sources of ohmic losses, which need to be minimized *via* specific cell designs and optimization of the electrolyte composition to maximize their energy efficiencies.[10] An important recent breakthrough in the development of flow cells is that the catalyst is deposited onto a gas diffusion layer (GDL) and the resulting gas diffusion electrode (GDE) is fed with CO_2 gas, resulting in high CO_2 coverage on the catalyst and industrially relevant current densities (several hundred mA cm^{-2} up to A cm^{-2}). In the classical H-cells, the electrolyte is saturated with CO_2 and the low CO_2 concentration in water (30 mM) results in mass transport limitations and much lower current densities (below 50 mA cm^{-2}). The technological issues related to the electrolyzer have been extensively presented in several recent review articles, and thus will not be discussed here.[11–13]

Catalysis is a critical component of this technology for optimizing the reaction kinetics and selectivity. CO_2R involves multi-electron and multi-proton reactions, with electrons coming from the cathode and protons from the aqueous electrolyte.

These reactions are associated with large overpotentials and low kinetics, deteriorating the energy efficiency. Thus, catalysts, which facilitate the transfer of electrons and protons, are required to minimize these barriers.[14,15] Furthermore, a variety of products can be obtained by the addition of electrons and protons to CO_2, within a limited potential range (Table 1). The selectivity can be controlled by tailoring the electronic and structural properties of catalysts. It should be noted that the hydrogen evolution reaction (HER) *via* proton reduction always competes with CO_2R, and thus catalysts have also been developed to minimize HER. Obviously, the carbon number increase in more complex product molecules, requiring more electrons and protons to be transferred, which results in larger overpotentials, and hence slower reaction kinetics and low selectivity. This explains why CO_2R to C_1 products, such as carbon monoxide and formic acid,[16,17] is more industrially mature than CO_2R to C_2 products, such as ethylene and ethanol, and the formation of C_{3+} products (see some examples in Table 1) is more challenging, and thus rarely observed at low current densities and with low faradaic efficiencies. Previous articles reviewed the field of CO_2R to C_2 compounds (namely ethylene, acetate and ethanol).[8,18,19] Thus, the focus of this review article is on the recently discovered catalysts allowing production of complex C_{3+} organic molecules from CO_2R, and also from COR.

The selectivity can be controlled based on the choice of the metal used at the cathode.[20] The majority of metals (Pt, Pd, Rh, Fe, Ni, Co, *etc.* favor HER over CO_2R. Alternatively, Ag, Au and Zn, to a low extent, are well known to favor CO production, which is a C_1 product obtained *via* the 2-electron reduction of CO_2. Sn, Bi and In are selective for formic acid production, which is also a C_1 product obtained *via* 2-electron reduction. Although methanol is rarely observed, methane, another C_1 product, can be obtained with a very high faradaic efficiency using Cu-derived catalysts.[21] Cu is considered a unique catalyst, given that it is frequently claimed to be the only metal capable of promoting C–C coupling reactions. As demonstrated herein, this is not correct given that other metals can also promote these reactions. It should be noted that the Cu-dependent CO_2R

Table 1 CO_2R-derived products and the corresponding half-reaction redox potentials (*vs.* RHE)

	Products	Half reaction	E^0 (V *vs.* RHE)
	Hydrogen	$2e^- + 2H^+ \rightarrow H_2$	0.00
C_1	Formic acid	$CO_2 + 2e^- + 2H^+ \rightarrow HCOOH_{(L)}$	−0.12
	Carbon monoxide	$CO_2 + 2e^- + 2H^+ \rightarrow CO_{(g)} + H_2O$	−0.1
	Methane	$CO_2 + 8e^- + 8H^+ \rightarrow CH_{4(g)} + H_2O$	0.17
C_2	Ethylene	$2CO_2 + 12e^- + 12H^+ \rightarrow C_2H_{4(g)} + 4H_2O$	0.08
	Ethanol	$2CO_2 + 12e^- + 12H^+ \rightarrow C_2H_5OH_{(L)} + 3H_2O$	0.09
	Ethane	$2CO_2 + 14e^- + 14H^+ \rightarrow C_2H_{6(g)} + 4H_2O$	0.14
	Ethylene glycol	$2CO_2 + 10e^- + 10H^+ \rightarrow C_2H_6O_{2(L)} + 2H_2O$	0.2
	Acetic acid	$2CO_2 + 8e^- + 8H^+ \rightarrow C_2H_4O_{2(L)} + 2H_2O$	0.11
C_3	Propanol	$3CO_2 + 18e^- + 18H^+ \rightarrow C_3H_7OH_{(L)} + 5H_2O$	0.1
	Acetone	$3CO_2 + 16e^- + 16H^+ \rightarrow C_3H_6O_{(L)} + (H_2O$	−0.14
	Propylene	$3CO_2 + 18e^- + 18H^+ \rightarrow C_3H_{6(g)} + 6H_2O$	0.13
	Propane	$3CO_2 + 20e^- + 20H^+ \rightarrow C_3H_{8(g)} + 6H_2O$	0.14
C_4	Methyl glyoxal	$3CO_2 + 12e^- + 12H^+ \rightarrow C_4H_4O_{2(L)} + 4H_2O$	0.02
	Butane	$4CO_2 + 26e^- + 26H^+ \rightarrow C_4H_{10(g)} + 8H_2O$	0.14
	Butanol	$4CO_2 + 24e^- + 24H^+ \rightarrow C_4H_{10}O_{(L)} + 7H_2O$	0.14
	2,3-Furandiol	$4CO_2 + 14e^- + 14H^+ \rightarrow C_4H_4O_{3(L)} + 5H_2O$	0.01

to multi-carbon compounds is generally limited to the generation of C_2 compounds such as ethylene and ethanol, whereas propanol is also formed in substantial yield in only a few circumstances, discussed in detail in a dedicated chapter. Because these reactions rely on a large number of electrons and protons, their mechanism is very complex, implying the involvement of a large number of surface adsorbed intermediates, and thus has been a matter of intense experimental and computational research.[22] Although this capacity makes Cu very attractive, generally Cu-based catalysts suffer from a lack of selectivity, and resulting in a complex mixture of a variety of C_1 (CO, HCOOH, and CH_4) and C_2 products (ethylene and ethanol) together with H_2. Accordingly, numerous strategies have been developed to better control the selectivity of Cu-based catalysts including tuning the morphology and size of nanoparticles, introducing defects, alloying and metal-doping, surface functionalization with molecules and polymers, and electrolyte engineering.[23,24]

CO_2R suffers from an additional drawback, namely the formation of carbonate/bicarbonate salts *via* the reaction between OH^- formed during the reaction and CO_2 dissolved in the electrolyte or at the gas-electrolyte interphase.[25,26] This results in unproductive CO_2 consumption, changes in the membranes and electrolyte, instability of the whole electrochemical system and extra costs associated with the recovery and recycling of the electrolyte as well as the recovery of CO_2. Thus, a strategy to limit the problem of CO_2 loss and carbonate formation is shifting from single-step to tandem CO_2R, involving the first step of CO_2R to CO, followed by COR to C_{2+} compounds using Cu-based catalysts.[27] The rational is based on the fact that CO does not react with OH^-, and thus highly alkaline electrolytes, favoring C–C coupling and suppressing HER, can be used in CO electrolyzers. Furthermore, given that high CO surface coverage favors C–C coupling, COR competes favorably with HER, and generally is more selective towards C_{2+} products than CO_2R, despite their lower water solubility.[28] Because of this very low solubility of CO in water, flow electrolyzers and GDEs for COR have been developed recently, showing remarkable achievements with respect to ethylene and ethanol production, with high selectivity at high current densities.[29,30] However, the tandem scenario requires that the CO_2-to-CO electrochemical step does not degrade CO_2 into carbonate too extensively. This is the case if a high-temperature solid oxide electrolysis cell (SOEC) is used for highly efficient and selective CO_2R to CO, given that it avoids carbonate formation.[27] A recent techno-economic benchmarking analysis indeed showed that this tandem system is the most economically promising for the production of ethylene due to the very high energy efficiency and excellent selectivity of already available systems for CO_2R to CO under conditions of limited CO_2 loss to carbonate.[31] Therefore, here we also discuss interesting catalysts for CO electroreduction (COR) to C_{3+} products.

An alternative strategy for limiting carbonate formation and carbon loss is the utilization of acidic electrolytes for CO_2R, although specific catalysts have to be designed for limiting

HER.[32,33] However, the specific conditions will not be discussed here given that, to our knowledge, there is no report of significant C_{3+} product formation during acidic CO_2R.

Thus, the aim of this review is to summarize the current knowledge regarding solid catalysts specifically promoting the formation of C_{3+} products containing three carbon atoms or more during both CO_2R and COR. Remarkably, as expected, most reports focused on Cu-based catalysts; however, a significant number of studies showed the potential of other transition metals for catalyzing the formation of these complex molecules, although with low faradaic efficiencies (FEs) and low current densities. It is important to appreciate the development of highly sensitive analytic methods (NMR, gas and liquid chromatography), which has allowed the detection of very low amounts of products (with faradaic efficiencies as low as 0.1%), although in some cases, the detection of the products was only possible *via* long-term electrolysis and the use of large cathodes.

Considering the industrial importance, with increasing demand and high potential growth rate, of some C_{3+} compounds, such as propanol, propylene, propane, butane and butanol, it is worth focusing on these reactions as a sustainable alternative way to produce them. These compounds are indeed key precursors of polymers, fuels and rubber, making them attractive targets for CO_2R and COR. The most important C_3 and C_4 organic chemicals according to their market volume are shown in Table 2.

Based on the data analyzed here, we present a full view of the C_{3+} products accessible *via* CO_2R and COR and a comparison

Table 2 Market size of some C_{3+} compounds

Products	Volume (2023) millions of tons	USD billion (2023)	Expected growth rate (%) 2023–2032	Data source
Propylene	100	121	5.4	a
Propanol	3.2	4.2	7.0	b
Propane	189	98	12.5	c
Acetone	8.1	6.5	3.8	d
Butanol	5.5	9	6.2	e
Butane	200	112	4.1	f
Butene-1	3	3.2	3.7	g
Propylene oxide	10	23.5	5.8	h
Butadiene	12	12.1	4.7	i

[a] The data are obtained from: **https://www.chemanalyst.com/industry-report/propylene-market-633**. [b] The data are obtained from: **https://www.chemanalyst.com/industry-report/isopropyl-alcohol-ipa-187**. [c] The data are obtained from: **https://www.mordorintelligence.com/industry-reports/propane-market**. [d] The data are obtained from: **https://www.statista.com/statistics/1245205/acetone-market-volume-worldwide/**. [e] The data are obtained from: **https://www.statista.com/statistics/1245211/n-butanol-market-volume-worldwide/**. [f] The data are obtained from: **https://www.globalinsightservices.com/reports/butane-market/**. [g] The data are obtained from: **https://prismaneconsulting.com/report-details/butene-1-market-insights-trends-analysis-and-forecast#:~:text=Butene-1%20Capacity%20Overview,number%20of%20on%20purpose%20capacity**. [h] The data are obtained from: **https://eippcb.jrc.ec.europa.eu/sites/default/files/2019-11/JRC109279_LVOC_Bref.pdf**. [i] The data are obtained from: **https://www.statista.com/statistics/1067436/global-butadiene-production-capacity/#:~:text=The%20production%20capacity%20of%20the,additions%20in%20the%20next%20years**.

with the list of industrially relevant compounds, providing a rational perspective regarding the reactions that should be further studied and developed. We also provide a benchmarking of the different catalysts favoring the formation of these products in terms of their performances and catalytic mechanisms, opening new research directions with respect to the elaboration of catalysts for CO_2 and CO valorization. During the preparation and finalization of this article, a review article was published on a similar topic.[34] However, our approach is from a different perspective, and thus we believe that these two articles are nicely complementary.

1. Non-Cu-based catalysts

To our knowledge, only a few metals, the most interesting one being Mo, Ni and Fe, were reported as catalysts for C–C coupling reactions leading to multi-carbon compounds from CO_2R. Metal-free catalysts have also been reported to catalyze these reactions, and one example will be described at the end of this chapter. The few available reports are summarized in Table 3, presenting a list of the products and most relevant performances reflecting the activity of non-Cu catalysts, namely, Faraday efficiencies, applied potentials and geometric current densities (total or partial), under specific reaction conditions. In a few cases, the reaction mechanisms are proposed to explain the formation of a given product, but one should be aware that computational and experimental mechanistic validations are missing generally. It should also be noted that non-Cu catalysts have not been studied for COR to date, with the exception of silver under high CO pressure conditions (see Section 1.6).[35]

1.1. PdAu-based catalysts

The bimetallic PdAu material, obtained *via* the electrodeposition of Pd on an Au substrate, was shown to not only catalyze the electroreduction of CO_2 to formic acid as the main product but also a variety of multi-carbon products, essentially hydrocarbons, albeit with very low faradaic efficiencies (FEs < 1%) including C_2 (ethylene and ethane), C_3 (propane and propylene), C_4 (butane, 1-butene and isobutene), and C_5 (pentane, pentene and 2-methyl-butane) (Table 3).[36] To the best of our knowledge, this was the first non-Cu-based material that showed the ability to catalyze C–C coupling reactions. Although no mechanistic study was provided in this report, it was proposed without experimental and theoretical support that the reaction proceeds *via* CO_2R to *CO, and then *CH_2 groups are adsorbed on the catalyst surface, followed by polymerization (*via* *CH_2–*CH_2 coupling), in agreement with the absence of oxygenates in the product mixture. In the following, an asterisk associated with a molecular formula, such as *CO, indicates that the molecule, here CO, is adsorbed on the surface of the solid catalyst. This putative mechanism is similar to the polymerization mechanism occurring in the Fischer–Tropsch (F–T) process.[48,49] In this case, the reaction of CO with H_2 (syngas) over a thermal catalyst at high temperature and

pressure involves the adsorption of *CO and dissociative adsorption of H_2, leading to the adsorption of *H. These two primary intermediates react *via* C hydrogenation and C–C_n coupling steps, leading to the formation of long-chain hydrocarbon products. During the electroreduction of CO_2, the same intermediates, *CO, coming from CO_2R, and *H, coming from H^+/H_2O reduction, are formed and can potentially proceed along comparable pathways. However, thus far, C–C_n coupling is limited to low n values and the production of long-chain hydrocarbons is not considered in general competitive with respect to H_2 formation and to CO desorption owing to its very low FEs (<1%).

1.2. Mo-based catalysts

Mo-based materials have been rarely used for CO_2R/COR. In contrast, MoS_2 is one of the most studied catalyst for proton electroreduction given that it has been proven to proceed with very low energy barriers and overpotentials.[50] Actually, when implemented in an H-cell containing a CO_2-saturated potassium phosphate electrolyte, H_2 was the major product. However, interesting organic products were observed, albeit in very low amounts and at very low current density (0.6 mA cm^{-2}) including 1-propanol (FE = 4%), ethylene glycol (FE: 0.65%) and *t*-butanol (FE = 0.2%) (Table 3).[37] These reactions were not studied further and no experimental and computational insight was provided into the understanding of the C–C coupling pathways on the surface of MoS_2.

In 2023, M. Asadi and coworkers reported a study showing that molybdenum phosphide, Mo_3P, has the potential to catalyze CO_2R with remarkable selectivity towards propane, achieving a very high FE of 91% using a flow cell with the catalyst deposited on a GDL at a high applied current density of 390 mA cm^{-2} during 100 h electrolysis (Table 3).[38] The observed selectivity and stability were attributed to the combination of the following factors: (i) surface functionalization with a monolayer of imidazolium molecules *via* electrodeposition and (ii) coating the GDE with an anion-exchange ionomer, which suppressed HER and helped maintain the molecular layer during long-term electrolysis. Alternatively, the bare Mo_3P material produced a mixture of CO (FE = 75%) and CH_4 (FE = 24%) under the same electrolytic conditions. The experimental and computational studies suggested that the active sites were the Mo atoms and that the presence of an imidazolium layer on Mo_3P decreased the charge-transfer resistance, favored *CO_2 adsorption *via* electrostatic interactions/H-bonds, stabilized *CO adsorption and promoted *CO coverage, favoring C–C coupling. These results are in agreement with the *in situ* electrochemical Raman spectroscopy results, showing high *CO coverage. However, this work did not provide any clue regarding the high selectivity for propane formation. DFT calculations showed a favorable mechanistic pathway from CO_2 to propane, implying an intriguing trimerization step, *CO + *CH + *CO → *CO − CH −CO, with a quite low energy barrier. They also suggested that the surface was carbophilic enough to stabilize *C intermediates on the surface and favor

Table 3 Non-Cu solid materials for CO_2R to C_{3+} products

Catalyst	Conditions	Applied total current density[a] Potential vs. RHE	Products	FE (%)	Ref.
PdAu	H-cell	−1.4 V[b]	C_2 (ethylene + ethane)	0.7	36
			C_3 (propene + propane)	0.3	
	0.1 M KPO_4		C_4 (butene + butane + isobutene)	0.16	
			C_5 (pentene + pentane + 2-methyl-butane)	0.07	
MoS_2	H-cell	0.6 mA cm^{-2}	1-Propanol	4	37
	0.1 M KPO_4, pH 6.8	−0.6 V	Ethylene glycol	0.65	
			Tert-Butanol	0.2	
Mo_3P-Im	Flow cell	390 mA cm^{-2}	Propane	91	38
	1.0 M KOH				
Ni_3Al	H-cell	2.1 mA cm^{-2}	1-Propanol	2	39
	0.1 M K_2SO_4, pH 4.5				
Ni_2P	H-cell	<0.5 mA cm^{-2}	Methyl glyoxal	25	40
	0.5 M $KHCO_3$, pH 6.8		2,3-Furandiol	71	
NiP_2	H-cell	<0.5 mA cm^{-2}	Methyl glyoxal	84	40
	0.5 M $KHCO_3$, pH 6.8		2,3-Furandiol	15	
Ni_2P–CTAB	H-cell	0.8 mA cm^{-2}	Methyl glyoxal	97	41
	0.5 M $KHCO_3$, pH 6.8		2,3-Furandiol	1	
	Flow cell	50 mA cm^{-2}	Methyl glyoxal	50	
	0.4 M K_2SO_4	200 mA cm^{-2}	Methyl glyoxal	40	
Ni_2P-Ho_2O_3	H-cell	0.95 mA cm^{-2}	Acetone	25.4	42
	0.1 M $KHCO_3$, pH 6.8				
Ni phosphate	Flow cell	12 mA cm^{-2}	Propene	2.2	43
			Propane	1.2	
			1-Propanol	0.5	
			1-Butene	0.8	
			Iso-butane	0.3	
	0.1 M $KHCO_3$, pH 6.8		n-Butane	0.3	
			1-Butanol	0.3	
			1-Pentene	0.5	
			n-Pentane	0.2	
			n-Hexane	0.16	
Ni-doped $(Cr_2O_3)_3Ga_2O_3$	H-cell 0.1 M KH_2PO_4/0.1 M K_2HPO_4, pH 6.7	−0.88 V 0.2 mA cm^{-2}	1-Butanol 3-Hydroxy butanal	42 5	44
AuNi	H-cell	2 mA cm^{-2}	C_nH_{2n}	0.12	45
	0.1 M $KHCO_3$, pH 6.8		C_nH_{2n+2} (n > 2)		
Fe_2P	H-cell	<1.0 mA cm^{-2}	Methyl glyoxal	20	46
	0.5 M $KHCO_3$, pH 6.8		2,3-Furandiol	8	
Co_3O_4	Flow cell	29.8 mA cm^{-2}	C_2–C_7 hydrocarbons	0.56	47
	0.1 M $KHCO_3$	−0.9 V vs. RHE			

[a] Partial current density can be derived from the total current density (column 3) with the FE for a given product (column 5). [b] The information regarding current density is not available.

dehydration, in agreement with the lack of oxygenates.[51] This class of materials clearly deserves further investigation.

1.3. Ni-based materials

Up to recently, Ni was not expected to promote C–C coupling from CO_2R, where Hori and collaborators earlier described CO poisoning of Ni surfaces, leading to their generally high catalytic activity for HER.[52] Nevertheless, the theoretical study by Norskov and collaborators predicted that Ni–Ga alloys can catalyze CO_2R.[53] Subsequently, N. Lewis and collaborators demonstrated CO_2R to methane, ethylene and ethane using different phases of Ni–Ga as catalysts; however quite inefficiently, with very low FEs (below 2%) and low current densities.[54] A. B. Bocarlsy extended this study to Ni–Al materials and reported that Ni_3Al thin films supported on glassy carbon could catalyze the formation of a variety of C_1, C_2 and also C_3 products from CO_2R, providing, to our knowledge, the first illustration of an Ni-based material capable of promoting

C–C coupling from CO_2 up to a C_3 product.[39] Although the major products of the reaction carried out under the conditions of 0.1 M CO_2-saturated K_2SO_4 and pH 4.5 were H_2 (FE > 60%) and CO (FE = 33%) at the optimal applied potential, giving a current density of 2.1 mA cm^{-2}, 1-propanol was the major liquid product (FE = 2%), together with minor amounts of methanol, formate, ethanol (FE < 1%) and traces of acetone (Table 3). This system proved remarkably stable during several days of electrolysis. However, although preliminary mechanistic studies indicated that CO is a key intermediate, no further chemical study was provided regarding how Ni_3Al facilitates the formation of C_3 products (propanol and acetone).

Despite the fact that nickel phosphides were reported as highly active HER catalysts, G.C. Dismukes and collaborators discovered that they could also be used as electrocatalysts for CO_2R.[40] In their study, different nickel phosphide compounds (Ni_3P, Ni_2P, Ni_2P_5, Ni_5P_4 and NiP_2) were synthesized and deposited on an aluminium die as a working electrode support

within an H-cell electrolyzer. Remarkably, CO_2 electrolysis led to the production of multi-carbon oxygenates, such as methylglyoxal, a C_3 product, and 2,3-furandiol, a C_4 product; however, only when a very low potential of -0.1 V $vs.$ reversible hydrogen electrode (RHE) (thus with a very low current density, < -0.5 mA cm^{-2}) was applied. The most selective catalyst for methylglyoxal was NiP$_2$, with an FE of 84% at -0.10 V $vs.$ RHE, while the maximum FE for 2,3-furandiol was 71% observed at 0 V $vs.$ RHE on Ni$_2$P (Table 3). At slightly more cathodic potentials (< -0.2 V $vs.$ RHE), the reaction selectivity shifted to HER. Although formic acid was produced at all potentials, FE$_{formate}$ never exceeded 5% for any of the Ni phosphides. With these low cell potentials, high energy efficiency values were obtained, namely 99% and 92%, for Ni$_2$P and NiP$_2$, respectively. The authors observed a preference for P-rich Ni phosphides in forming C_3/C_4 products, suggesting that the nucleophilic surface P sites are the potential binding sites for hydridic *H and *CO_2.

Regarding the mechanisms, the low potentials, close to equilibrium potentials, at which product formation takes place exclude CO_2 adsorption, followed by activation via proton-coupled electron transfer, which requires much more cathodic potentials (-0.7 to -1.0 V $vs.$ RHE). This suggests a hydride transfer mechanism (Fig. 1) in the initial rate-determining step during CO_2 conversion to formic acid. Regarding the formation of multi-carbon products, the system is quite intriguing, considering the nature of the products, methylglyoxal and 2,3-furandiol, highly oxygenated compounds, and the absence of CO formation, which excludes *CO–*C_n coupling pathways for chain elongation as in the case of Cu-based catalysts (see Section 2). Based on thermodynamic considerations, it has been proposed that the reaction proceeds via a series of aldehyde self-condensation steps (Fig. 1). The reaction would

start from surface adsorbed formaldehyde, which is derived from formic acid reduction by a hydride species, giving rise to adsorbed glycoaldehyde, then adsorbed glyceraldehyde (from the condensation of formaldehyde with glycoaldehyde), and finally methylglyoxal (from the condensation of formaldehyde with glyceraldehyde) (Fig. 1). Thus, methylglyoxal is proposed to be derived from the condensation of three formaldehyde molecules. 2,3-Furandiol is formed by the last condensation between methylglyoxal and formaldehyde, followed by furan five-membered cycle formation and hydride abstraction for ring aromatization. There is precedent in the literature for hydride abstraction by nickel phosphides.[55] It was proposed that these aldehyde condensation reactions are catalyzed by Ni phosphides, which display favorable Lewis acid character (given that carbonyl binding to a Lewis acid surface lowers the barrier for proton abstraction from the C–H of formaldehyde), and furthermore, as mentioned, Ni phosphides also favor the last hydride abstraction.[55] Thus, the proposed mechanism is dependent on two initial successive hydride transfers to produce formate, and then formaldehyde and with formic acid/formaldehyde, leading to multi-carbon products, which greatly differs from the CO_2R mechanism on Cu-based catalysts (see Section 2). This was supported by experiments using the intermediates (formate, formaldehyde, and methylglyoxal) as substrates in the absence of CO_2. A computational study established the key role of Ni-bound surface-adsorbed hydride H* species (bound at an Ni$_3$ hollow site) in the formation of formic acid, and then formaldehyde.[56] However, the strong affinity for surface H* is responsible for the large kinetic barrier for these two first steps (>1 eV), limiting the catalytic activity of Ni$_2$P, which is consistent with the very low turnover frequency observed. It also shown that H$_2$CO* self-coupling giving glycoaldehyde is thermodynamically downhill by 0.41 eV, and thus
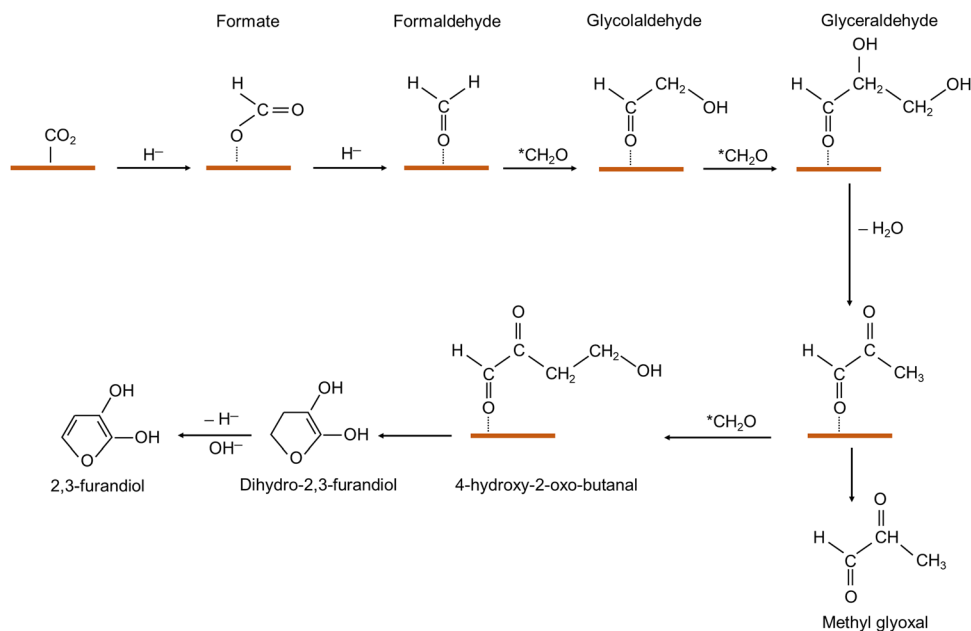

Fig. 1 Proposed mechanism for methyl glyoxal and 2,3-furandiol formation catalyzed by nickel phosphides.[40]

more favorable than the further reduction of adsorbed formaldehyde to C_1 products (CH_3OH and CH_4) displaying high kinetic barriers. Glyceraldehyde formation *via* coupling glycoaldehyde and a third molecule of H_2CO^* and the subsequent water elimination giving 2-hydroxy-2-propenal are also downhill by 0.19 and 0.96 eV, respectively. Finally, the formation of methylglyoxal (enol–keto tautomerization) is downhill by 0.31 eV, while the formation of the C_4 molecule, furandiol, is nearly thermoneutral. Thus, the overall energetics of the proposed mechanism is strongly exergonic, with the formation of surface hydrides being essential, and with the first step of hydride transfer to CO_2 being the rate-limiting step. Thus, this is the key target to study and optimize to improve the catalytic activity *via* active site engineering.

Dismukes and collaborators achieved a remarkable improvement in the system performances by combining the following: (i) a high surface area Ni_2P material (Ni_2P–CTAB) with a much larger surface density of catalytic sites, owing to a specific soft-templating synthesis procedure using a surfactant, cetyltrimethylammonium bromide (CTAB), to control the material morphology; (ii) surface modification of the catalyst with a hydrophobic anionic polymer (PFAEM) as a co-catalyst binder to increase the CO_2R vs. HER selectivity; and (iii) a flow cell with a GDE to improve CO_2 mass transport to the catalyst and limit HER under larger current densities.[41] Indeed, the use of an H-cell system allowed remarkably high FE for methylglyoxal (97%) at applied potentials close to the RHE, at very low current densities (Table 3). Instead, with a flow cell system based on a bipolar membrane, high total current densities in the range of 50 to 200 mA cm^{-2} could be applied, while achieving remarkably high FE for CO_2-derived products, almost exclusively methylglyoxal, accounting for a total FE of up to 40–50%. The control experiments showed that Ni_2P, in contrast to Ni_2P–CTAB, produced only H_2 at the applied current densities, under the same electrolytic conditions.

Ni_2P was also studied as a part of pure monodisperse core/shell nanoparticles (CSNPs), in which the inner core was made of crystalline Ni_2P and the 1.3 nm-thick outer shell was made of amorphous Ho_2O_3.[42] The amorphous shell was designed to provide a high density of active sites, defects, and undercoordinated sites, while the crystalline conductive core facilitated charge transfer between the core and shell. This material behaved as a catalyst; however, it was not stable for CO_2R in an H-cell using CO_2-saturated 0.1 M $KHCO_3$ as the electrolyte, leading to the large production of acetone (FE = 25.4%) at an applied potential of −0.98 V vs. RHE (total current density 0.95 mA cm^{-2}), together with H_2 as the main product (FE > 60%), HCOOH and CH_3OH (Table 3). Coupling between the $^*C_1$ and $^*C_2$ intermediates was proposed for the formation of the C_3 product acetone, but owing to the lack of mechanistic studies, it is difficult to understand why only acetone is formed as a C_{2+} product given that no C_2 product and no propanol were observed.

Inorganic nickel oxygenates (nickel phosphate, nickel carbonate, nickel bicarbonate, nickel hydroxide and nickel oxide), deposited on a GDL, were also shown to catalyze CO_2R in a flow cell electrolyzer, using a 0.1 M $KHCO_3$ electrolyte and an applied potential of −1.0 V vs. RHE.[43] Remarkably, while H_2 was the major product (FE = 65%), a great variety of CO_2-derived carbon compounds was detected. These compounds not only included C_1 (CO, formate, and methane), with a total FE of 13.5%, and C_2 (ethylene, ethanol, and acetaldehyde), with a total FE of 6%, products usually found in Cu-catalyzed CO_2R, but also a long list of C_3, C_4, C_5 and C_6, linear and branched, products. In the case of the most productive catalyst, namely Ni phosphate, C_{3+} hydrocarbon products accounted for a total FE of 6.5% with a partial current density of 0.91 mA cm^{-2}, while lower amounts of oxygenates (FE = 3.8%), including alcohols up to C_4 (1-butanol), were detected. Nevertheless, each product accounted for FE < 2%, with the C_{3+} products being propene (2.2%), propane (1.2%), 1-propanol (0.5%), 1-butene (0.8%), isobutene (0.3%), *n*-butane (0.3%), 1-butanol (0.3%), 1-pentene (0.5%), and *n*-pentane (0.2%) (Table 3). The heaviest compound and unique C_6 compound was *n*-hexane (FE = 0.16%).

Using *operando* X-ray absorption near edge structure (XANES), it was observed that unlike Cu systems, the inorganic Ni oxygenates do not undergo full reduction to metallic Ni, where the absorption of the Ni K-edge indicated the existence of stable $Ni^{\delta+}$ sites. The presence of Ni^{2+} was proposed to be due to the retention of (near)-surface oxygenated species and stable Ni–O bonds, as shown by *operando* EXAFS. This might explain why CO is moderately bound at the catalyst surface compared to Ni^0, freeing it from CO poisoning, a characteristic of metallic Ni, and allowing further COR and C–C coupling. This was confirmed by density functional theory (DFT) calculations using surface models with a wide degree of polarization owing to O or OH doping, which showed that the CO binding strength was weakened and C–C coupling favored on surfaces with increased positively charged Ni sites. Considering the extreme complexity of the reactions, implying a huge number of electrons and protons for the formation of each of the C_4–C_6 products, and thus a huge number of possible intermediates (hundreds), the mechanism is almost impossible to decipher. Nevertheless, it was proposed that $^*CH$ and $^*CH_2$, derived from CO or CH_2O, respectively, were the key species in C–C coupling reactions, leading to an extension of the carbon chains during the formation of long-chain hydrocarbons. In this work, according to the proposed mechanism, the first C–C bond formation on the polarized Ni surface proceeds *via* the $^*CH/^*CH_2$ + $^*COOH$ coupling pathway, followed by $^*CH$ and $^*CH_2$ insertions to form C_{3+} hydrocarbons. Recently, M. T. M. Koper's group reported further information regarding this Ni phosphate material.[57] They showed that while the effect of temperature and pressure on selectivity towards long-chain hydrocarbons was minor, the catalyst was more sensitive to variations in the electrolyte composition, with K^+ cations and better proton-donating anions, such as phosphate, favoring long-chain hydrocarbons.

A study in 2023 confirmed the ability of Ni to promote C_{3+} product formation.[44] Ni-doped $(Cr_2O_3)_3Ga_2O_3$ was indeed shown to catalyze the electroreduction of CO_2 to 1-butanol, with a remarkable FE of 42%, during 20 h electrolysis at an

applied potential of -1.48 V *vs.* Ag/AgCl; however, at low current density of <1 mA cm^{-2} using an H-cell containing KCl/NaHCO$_3$ as the electrolyte at pH 4 (Table 3). 3-Hydroxybutanal, a C$_4$ product, was also obtained with an FE of 5% (FE of 25% was obtained at pH 5 with an applied potential of -1.4 V). Acetic acid was also detected (FE = 9%). In contrast, dopant-free (Cr$_2$O$_3$)$_3$Ga$_2$O$_3$ produced mostly hydrogen (FE$_{H2}$ = 92%), with very minor amounts of CO$_2$-derived products, such as acetic acid, acetaldehyde and acetone. As a control experiment, all the products previously identified with the Ni-doped (Cr$_2$O$_3$)$_3$Ga$_2$O$_3$ catalyst were detected after 20 h electrolysis of formic acid used as the substrate in place of CO$_2$. This supported the hypothesis that formate could serve as the primary intermediate towards multi-carbon compounds, a mechanism similar to that proposed for Ni phosphides.[40] Acetaldehyde was also proposed to be a secondary intermediate given that the electrolysis of acetaldehyde using Ni-doped (Cr$_2$O$_3$)$_3$Ga$_2$O$_3$ resulted in the production of 1-butanol. (Cr$_2$O$_3$)$_3$-Ga$_2$O$_3$ was proposed as the source of acetaldehyde and nickel atoms as the critical component for acetaldehyde conversion to butanol given that the electrolysis of acetaldehyde using a coiled Ni wire or a planar glassy electrode electroplated with Ni resulted in the formation of significant amounts of 1-butanol. In conclusion, according to the proposed mechanism, the catalyst activates surface hydrides to allow the conversion of CO$_2$ to formic acid and its reduction to formaldehyde, which couples with a second molecule of formaldehyde to form acetaldehyde. Thus, this step is thus facilitated by (Cr$_2$O$_3$)$_3$-Ga$_2$O$_3$. Then, the Ni sites promote the coupling of two molecules of acetaldehyde to generate 3-hydroxybutanal, which is then further reduced to 1-butanol (Fig. 2).

Finally, the recent report on an Au–Ni catalyst leading to the formation of long-chain hydrocarbons should be mentioned.[45] Following the concept that the F–T mechanism could operate during CO$_2$R with an appropriate combination of metals, providing *CO and *H intermediates (see Section 1.1), the Au–Ni material, synthesized *via* Au deposition on an Ni sheet,

was chosen for the following reasons. Ni served to enhance CO adsorption and favor surface *H coverage, while Au was selected for generating a high surface density of *CO. Under these favorable conditions, *CO and *H could combine to form *CH$_x$ and promote *C$_1$–*C$_n$ polymerization steps. Actually, besides the large production of H$_2$ and CO, a series of C$_n$H$_{2n+2}$ and C$_n$H$_{2n}$ products, up to n = 7, was detected, including isomers of butane (isobutane and 2-methylpropane) and pentane (isopentane and 2-methylbutane) during CO$_2$R in an H-cell at a potential of -0.977 V *vs.* RHE using 0.1 M KHCO$_3$ as the electrolyte. No liquid products were detected. Nevertheless, the total FEs for these hydrocarbons were very low (FE = 0.23%, with small variations depending on the applied potential and the Au thickness) at a total current density of about 2 mA cm^{-2} and with the C$_2$ products C$_2$H$_4$ and C$_2$H$_6$ accounting for about half of total FE (FE$_{C_2}$ = 0.11%, FE$_{C_2H_6}$ = 0.07%, and FE$_{C_2H_4}$ = 0.04%). In the absence of the Au deposit, hydrocarbons were also detected but with even lower total FEs ($<0.02\%$). The production of alkanes was much higher than alkenes. The same products were obtained during COR; however, with lower FEs. The product distribution was interpreted as an indication for a C–C coupling polymerization reaction mechanism, leading to long-chain hydrocarbons, similar to the conventional F–T synthesis.[48,49] The same products, also with a low FE of about 0.35% for C$_2$–C$_5$ hydrocarbons, were obtained using a Cd electrode but the FE increased to 0.45% upon modification by sputter deposition of Ni (FE also increased with Pt or Ag deposition).[58,59]

Besides the findings described above, it is interesting to mention a recent work confirming the ability of Ni-based materials to catalyze CO$_2$R to multi-carbon compounds.[60] In this case, a stable material composed of Ni particles encapsulated in N-rich carbon nanotubes was proven to be remarkable for converting CO$_2$ selectively to ethanol, a unique liquid product, and CO with very little production of H$_2$ (FE $<10\%$) using both H-cells and flow cells equipped with GDEs. Thus, it was possible to achieve FE values for ethanol in the
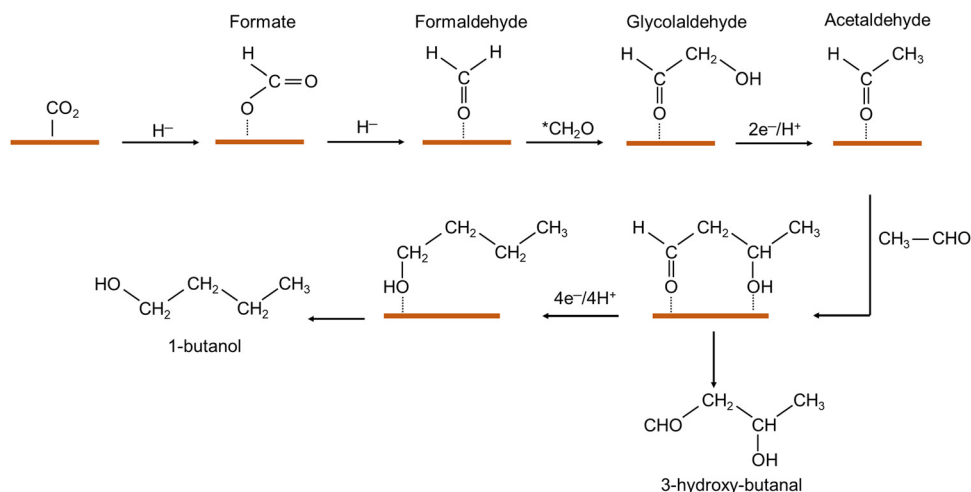

Fig. 2 Proposed mechanism for 1-butanol formation catalyzed by Ni-doped (Cr$_2$O$_3$)$_3$Ga$_2$O$_3$.[44]

range of 30–40%, within a wide voltage range of −0.6 to −1.2 V *vs.* RHE, enabling high current densities to be obtained (from 12 mA cm^{-2} in an H-cell to 127 mA cm^{-2} in a flow cell).

1.4. Fe-based catalysts

Based on a previous study on nickel phosphides, it was reasoned and confirmed computationally that iron phosphides, displaying weaker binding, and thus greater reactivity of surface hydrides, should catalyze CO_2R at greater rates.[46] Two initial reports indeed showed the ability of iron phosphides to catalyze C–C coupling specifically towards the formation of ethanol. Firstly, an FeP nanoarray on Ti mesh was shown to be able to catalyze CO_2R to methanol (FE = 80%) and ethanol (FE = 14%); however, at very low applied potentials (close to the onset potentials) and low current densities (~ 1 mA cm^{-2}) in 0.5 M KHCO$_3$.[61] Secondly, an Fe$_2$P$_2$S$_6$ sheet was shown to favor ethanol formation with a maximum FE of 23.1%; however, at even lower current densities (<0.5 mA cm^{-2}).[62] Later, another class of Fe-based catalysts with a core–shell architecture, with a nitrogen-doped γ-Fe$_2$O$_3$ material as the core and carbonitride as the shell, was also shown to catalyze CO_2R to a C$_2$ product, namely ethane, reaching an FE value of 42% at a significant current density of 32 mA cm^{-2} in an H-cell using a mixture of an ionic liquid, organic solvent (acetonitrile) and water as the electrolyte.[63]

Interestingly, a study confirmed the ability of Fe$_2$P to catalyze C–C coupling reactions, allowing CO_2 conversion to C$_3$ and C$_4$ products.[46] In contrast, Fe$_2$P could not catalyze COR, where CO essentially behaved as a poison. In 0.5 M KHCO$_3$, CO_2 electrolysis, at a very low applied potential (0.00 V) and low current density (<0.1 mA cm^{-2}), resulted in the production of formic acid (FE = 15%), methylglyoxal (FE = 20%), ethylene glycol (FE = 10%) and 2,3-furandiol (FE = 8%), the major product being H$_2$ (Table 3). The total FE for CO_2R products decreased upon applying more cathodic potentials (FE$_{max}$ = 53% at 0.00 V), with H$_2$ accounting for more than 95% at −0.2 V, but the maximum FE for ethylene glycol (22%) was obtained at −0.05 V. The proposed mechanism leading to methylglyoxal and 2,3-furandiol for Ni$_2$P was also applied in the case of Fe$_2$P, consisting of CO_2R to formate, and then to formaldehyde, from which C–C coupling occurs giving glycoaldehyde, then glyceraldehyde, and then methylglyoxal and furandiol *via* consecutive couplings with formaldehyde (Fig. 1). Ethylene glycol formation was proposed to proceed *via* the reduction of glycoaldehyde. The presence of this C$_2$ product in the case of Fe$_2$P and not Ni$_2$P is likely related to the greater reactivity of surface hydride on Fe$_2$P, favoring the C$_2$ pathway, which requires the addition of a hydride, while the C$_3$/C$_4$ pathway requires formaldehyde coupling. These experimental and computational studies indicate that surface hydrides and their binding affinities are potentially critical for promoting multi-carbon formation from CO_2.

1.5. Co-based catalysts

Based on the performances of inorganic nickel oxygenates[43] as well as the activity of Co-based catalysts for thermocatalytic CO hydrogenation and Fischer–Tropsch synthesis (FTS) reaction to produce long-chain hydrocarbons, a Co$_3$O$_4$ material was recently studied.[47] Co$_3$O$_4$ was deposited on carbon black, and then on a GDL of a three-compartment flow cell, and using a bipolar membrane, it could indeed catalyze the electroreduction of CO_2 into C$_2$–C$_7$ hydrocarbons (saturated and unsaturated including branched and linear isomers) during short term electrolysis, with the product distribution closely following the Anderson–Schulz–Flory distribution observed for thermocatalytic FTS. At an applied potential of −0.9 V *vs.* RHE in CO_2-saturated 0.1 M KHCO$_3$ as the electrolyte, the total FE for C$_{2+}$ products was 0.56% and the total partial current density was 0.12 mA cm^{-2}, with the major product being H$_2$ (Table 3). Co$_3$O$_4$ was the most active catalyst compared to CoO and Co oxygenates (phosphate, carbonate, and bicarbonate), while metallic Co only produced H$_2$. However, with prolonged electrolysis, the hydrocarbon production rate decayed as a consequence of a reduction-induced deactivation mechanism, following the accumulation of inactive metallic cobalt, as shown by *in situ* analysis of the catalyst under the operating conditions. Actually, upon reoxidation at an anodic potential of +0.6 V for 5 min, Co$_3$O$_4$ could be regained, and further CO_2 electrolysis showed that the catalytic capabilities to form long-chain hydrocarbons were recovered. CO was shown to be the primary coupling component and interfacial Co–Co$_3$O$_4$ centers were proposed to be the catalytically active sites. Indeed, DFT calculations showed that the *CO adsorption energy on these sites was comparable to metallic copper, and thus compatible with *CO activation for C–C coupling, in contrast to pure metallic Co (too strong adsorption energy leading to CO poisoning) or pure Co$_3$O$_4$ (too weak adsorption energy). DFT calculations also showed that chain elongation was more favorable *via* *CO–CH$_2$*, and then *CO–CH$_3$(CH$_2$)$_n$CH* coupling followed by termination *via* hydrogenation (reaction with H*), and furthermore that preference for chain growth over hydrogenation well explains the propensity of the interfacial sites to form long-chain hydrocarbons. This work demonstrated the possibility of using metal–metal oxide interfaces as an effective pathway towards CO_2R to long chain hydrocarbons, although the appropriate balanced population of each component may be difficult to control under the highly cathodic potentials used during CO_2R.

1.6. Ag-based catalysts

Ag is well-established as a catalyst for the selective formation of CO from CO_2R due to its low surface CO adsorption energy, and thus surface *CO desorbs faster than it reacts *via* C–C coupling. However, an interesting theoretical study suggested that Ag could have a lower onset potential for ethanol production from COR than that of Cu, suggesting that Ag can catalyze ethanol formation from COR if the surface CO coverage is sufficiently high.[64] This was confirmed a few years later using a pressure cell allowing alkaline COR to run under a high pressure of CO (from 10 to 60 bar) as a way to increase the CO coverage on the surface of a silver GDE.[35] Interestingly, very low amounts of C$_{2+}$ products were detected, predominantly oxygenates, in agreement with the DFT predictions, including C$_2$ products (ethanol,

acetic acid and ethylene glycol), and also a C_3 product, namely propanol. The largest amount of propanol was obtained at 60 bar (the total FE of the C_{2+} products was below 2% with a partial current density of < 8 mA cm^{-2}) and was proposed to be derived from the coupling reaction between CO and a surface-bound *C_2 oxygenated intermediate, likely to be one hydrogen short of acetaldehyde and precursor of ethanol as well. Thus, the product spectrum of Ag can resemble that of Cu under a high pressure of CO; however, at orders of magnitude lower formation rates.

Very recently, two other examples of Ag-based catalysts were shown to allow CO electroreduction to C_{2+} products. The first one was a PdAg alloy containing isolated Pd atoms.[65] This configuration allowed an increase in the *CO coverage owing to the presence of Pd atoms and a balance in the *CO adsorption energy, enabling C–C coupling to occur as in the case of Cu surfaces. Only C_2 products could be obtained (no C_3 product), such as ethylene, acetate and ethanol, with a total FE$_{C2}$ of 37% at -0.83 V vs. RHE and a partial current density of about 25 mA cm^{-2} in 1 M KOH. In the second example, it was found that the chirality-induced spin polarization of chiral nanostructured Ag films could promote *CO–*CO coupling during CO_2R in a pressure H-cell (P = 12.5 atm) in KHCO$_3$, leading, in addition to CO as the major product, to minor amounts of C_1 products (methane and methanol) and C_2 products (ethylene, ethane, acetate and ethanol) with only one C_3 product, propane, accounting for the maximum FE of about 1%.[66] The total FE$_{C2+}$ was 4.7% for a partial current density of 22 mA cm^{-2}.

1.7. Metal-free catalyst

A completely different approach was proposed recently, which is based on the ability of molecular metal-free frustrated Lewis acid–base pairs (FLPs) to activate CO_2, owing to electron donation from the lone pair of each O atom in CO_2 to the Lewis acid (LA) center and from the Lewis base (LB) to the C atom of CO_2.[67] A heterogeneous version of this concept, consisting of highly conductive graphene powder doped with boron atoms (6.8 at%) as LA and nitrogen atoms (4.2 at%) as LB, via the reaction of graphene with B and N dopants under high-frequency ultrasound, proved highly selective for propanol formation during CO_2R.[68] A record FE$_{propanol}$ of 50%, together with a high FE$_{ethanol}$, was obtained; however, in an H-cell system using 0.5 M Na$_2$SO$_4$ as the electrolyte at potentials more positive that -0.7 V vs. RHE, and thus at a very low total current density (2–6 mA cm^{-2}). A higher applied cathodic potential resulted in a large drop in FE$_{propanol}$. The control graphene doped with only one heteroatom, B or N, gave only a mixture of formic acid, as the major product, and small amounts of CO and H$_2$, demonstrating that C–C coupling occurred at the B/N-co-doping sites. DFT calculations showed a thermodynamically favorable pathway (favorable reaction free energy and activation energy barrier) involving the following steps: (i) binding CO_2 in a bidentate mode with N–C and B–O bonds favoring CO formation remaining attached to the B,N-site and (ii) C–C coupling between the CO intermediate and a second molecule of CO_2. This coupling reaction is more favorable than CO–CO

coupling, owing to the cooperative effect of the electron enrichment on C in N–CO–B and the electron deficiency on C in CO_2. Thus, here, the mechanism is proposed to be different from that occurring in Cu-based materials, where the coupling of *C_1 intermediates with CO_2 is excluded in general. Furthermore, the absence of hydrocarbons as products and the high selectivity for alcohols (ethanol and propanol) was explained by the suppressed deoxygenation steps given that DFT calculations demonstrated the high stabilization of the C–O bonds in the *C_2 and *C_3 intermediates by B/N-sites.

2. Cu-based catalysts

Presently, it is well-established that Cu-based materials have the greatest potential to catalyze the reduction of CO_2 to multi-carbon molecules with significant faradaic efficiencies and partial current densities. Although C_2 molecules such as ethylene and ethanol are the major multi-carbon products, propanol, a C_3 product, is also generally formed to a large extent, as discussed below. In 2012, employing highly sensitive analytical methods, T. Jaramillo and collaborators reported that the product mixture derived from Cu-dependent CO_2R is in fact much more complex than earlier anticipated, containing 16 different CO_2 conversion products, notably with very low amounts of C_3 products. The heaviest compounds, such as propionaldehyde, allyl alcohol, glycoaldehyde, ethylene glycol, acetone and hydroxyacetone, accounted individually for FE $<$ 1%.[69] In a more recent study by the M. Koper group, glyoxal and 1,2-propanediol, with FEs between 0.5% and 1%, were added to the list.[70] In 2015, the formation of low amounts of other C_3 compounds (propane and propene) as well as a C_4 compound, butane, was reported.[71] The latter study reported the highest FE for propanol (8.7%) at that time but larger values were obtained later, as discussed in a specific chapter on propanol formation. To our knowledge, the first report of C_4 oxygenate formation during CO_2R catalyzed by a Cu-based catalyst was published in 2020.[72] These studies clearly established the general complexity of the reaction product mixtures from Cu-based CO_2R, and thus confirmed the lack of selectivity of Cu-based systems. In the following, we only discuss Cu-based systems of interest, specifically producing C_3, notably propanol, propane and propylene, and C_4, notably butanol, compounds with relatively large total FEs.

2.1. Mechanistic theoretical considerations

In the case of Cu, the mechanism of CO_2 conversion to multi-carbon compounds has been extensively investigated theoretically.[73–75] Specifically, several excellent review articles have appropriately discussed our current knowledge, regarding the mechanism for the formation of C_2 compounds, ethylene, ethanol and acetate.[8,76,77]

DFT calculations are a major component of most studies reported on CO_2R and COR as a way to identify the most relevant intermediates, understand reaction mechanisms and provide some rational with respect to the effect of the structure,

morphology and composition of catalysts on their activity and selectivity. This is an attractive approach given that tremendous progress has been achieved in the development of DFT methods for describing periodic solids. However, this field suffers from the excessively systematic use of DFT calculations of reaction free energies and activation barriers, as a type of requested exercise, which is not always accessible and relevant. The frequent lack of relevance is attributed to two reasons. Firstly, the reactions leading to C_2 products and C_{3+} products are greatly complicated, involving a large diversity of potential intermediates, most of them not observable experimentally, despite efforts to use, for example, *in situ* vibrational spectroscopy, which is the most appropriate for the detection and identification of CO-derived intermediates.[78–81] For example CO_2R to the C_2 products ethylene and ethanol, the most studied pathway, requires 12 electrons and 12 protons, respectively. Thus, combining C–C coupling steps, coupled H^+/e^- transfer steps and deoxygenation steps, and considering the multiple configurations in which the same intermediate binds to the catalyst surface, involve more than 30 possible intermediates.[8,77,82] Reduction to propanol, a pathway much less studied thus far, requires 18 electrons and 18 protons, and thus potentially involves much more intermediates.[83,84] In general, under these circumstances, for simplification, a very small population of these intermediates is considered for calculating the energetics of the critical C–C coupling steps leading to C_2 or C_3 products. The second reason for the irrelevance is due to the growing complexity of the structure and the composition of the catalysts, which are no longer a pure single-facet metal, making it difficult to model their surface appropriately, and thus a large gap exists between the real catalyst and the model, given that it is necessarily over-simplified to make it accessible to current computing tools and time. The complexity is even more challenging if one considers that the dynamic reconstruction of the catalyst surface during electrolysis, which is almost always systematically overlooked, due to the harsh reaction conditions (polarization at very high cathodic potentials, extreme pH sometimes and large concentration of salts). Consequently, the theoretical structural models used to calculate the reaction energies and characterize the reaction mechanism are often too far from the real structure of the experimentally studied solid catalyst, and thus the conclusions from these studies should be considered with great care, which is not always the case. It is even more problematic in studies where the DFT calculations are performed first as a way to rationally identify a potential catalyst target for a given

reaction, given that there is little chance that the synthesized material will possess a structure similar to the anticipated simple model. Nevertheless, if one uses DFT calculations with sufficient modesty for these complex catalysts and reactions, they are useful in providing some rational for understanding some observed experimental trends.

The theoretical efforts have made it possible to propose the mechanism and intermediates for CO_2R and COR to C_2 products catalyzed by Cu-based catalysts. Briefly, as shown in the simplified version in Fig. 3, the first key intermediate is *CO, adsorbed on the surface, which can dimerize into *OCCO, forming a C–C bond. Then, a series of coupled electron/proton transfer steps generate a variety of $*C_2$ intermediates up to a few ones at which the ethylene and ethanol pathways bifurcate. Regarding C_3 product formation specifically, the proposed mechanisms in general involve C–C coupling steps between the *CO and $*C_2$ intermediates given that the trimerization of $*C_1$ intermediates is excluded because of its too high energy barrier.[83,84] DFT calculations of the reaction energies and barriers either simply consider coupling between *CO and *OCCO[85,86] or, in some cases, between *CO or *CHO and a variety of the most likely $*C_2$ intermediates, such as *HCCH, *CCO, *CHCO, *CHCHO and $*CH_3CO$, for example. This is consistent with these reactions being the most feasible steps towards the formation of C_3 products on Cu(100).[83,84,87,88] However, it is still unknown which pathways are the dominant ones.

Recently, another important issue computationally addressed regards the control of the selectivity among C_{2+} products towards oxygenates, specifically alcohols, ethanol and propanol, with respect to hydrocarbons, in particular ethylene.[51,75] F. Abild-Pedersen *et al.* found that carbophilicity of the surface was a simple and primary guide to interpret the oxygenate/hydrocarbon selectivity, where more carbophilic surfaces stabilize the intermediates, favoring dehydration towards ethylene, while a carbophobic surface disfavors C-bonded reaction intermediates in the ethylene pathway. DFT calculations were performed to determine the adsorption energy of C*, as the descriptor of surface carbophilicity, confirming, for example, that Cu(111) was less carbophilic than Cu(100), thus disfavoring ethylene. Oxophilicity can also be considered, as probed based on the calculated adsorption free energy of OH*, given that an oxophilic surface will have good affinity for the surface O-bonded intermediates, species. These species are widely accepted as intermediates towards the formation of alcohols, but this parameter is less instrumental in
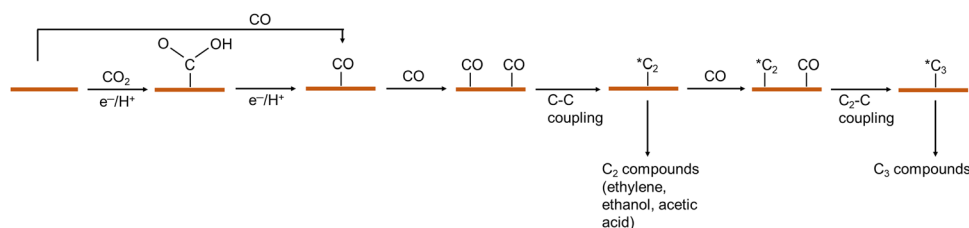

Fig. 3 Simplified mechanism for CO_2R showing the involvement of adsorbed *CO, $*C_2$ and $*C_3$ intermediates.[83]

discriminating between oxygenates and hydrocarbons.[51] A recent study using *in situ* surface-enhanced Raman spectroscopy (SERS) presented new insights into the specific Cu sites and surface intermediates that favor ethylene (intermediate *COCO) or ethanol (intermediate *OCHCH$_2$).[81]

In agreement with the importance of *CO for C–C and C–C$_2$ coupling, efforts have been devoted to elaborating Cu-based catalysts that favor CO coverage. This can be achieved in particular by tailoring the surface of the material by introducing grain boundaries, defects and undercoordinated sites.[8,89–97]

2.2. C$_3$ oxygenate formation *via* CO$_2$R and COR

Considering its high energy-mass density (30.94 kJ g^{-1}) and high octane number (118), the fuel efficiency of *n*-propanol is close to that of gasoline. Furthermore, it can be blended with gasoline to form a cleaner fuel. Finally, it is a precursor for the polymer industry, and thus it has a high market value. It is currently produced in the industry from fossil-derived ethylene *via* hydroformylation to propionaldehyde, followed by reduction. Propanol is almost systematically formed during CO$_2$R catalyzed by a variety of Cu-based materials, including polycrystalline Cu, albeit with low selectivity, namely with FEs lower than about 10%.[98–102] This suggests that Cu surfaces partially stabilize *C$_2$ intermediates enough to allow coupling with *C$_1$ intermediates, before the C$_2$ products desorb (Fig. 3). The recent study by M Koper and collaborators indeed nicely showed that a *CO trimerization mechanism is unlikely and that *n*-propanol formation can only be optimized *via* the fine balance of the relative surface coverage of CH$_3$–CO* methyl carbonyl (dehydrogenated acetaldehyde), a common possible *C$_2$ intermediate towards ethanol and propanol, and *CO, given that these two intermediates compete for the same active sites on the catalyst surface.[103] This explains why the selective formation of propanol is challenging given that HER is favored

at low *CO coverage, while at high *CO coverage, CH$_3$–CO* coverage and C$_1$–C$_2$ coupling are disfavored. Nevertheless, some interesting studies led to the development of selective, efficient and cost-effective catalysts for propanol formation using CH$_3$–CO* or CO electrolysis fueled by low-carbon electricity. Very few studies reported FE$_{propanol}$ exceeding 15%. Here, we exclusively discuss these systems.

2.2.1. Propanol from CO$_2$R (Table 4 and Fig. 4). Electrocatalytic CO$_2$R on single crystal Cu facets indicated that the (100) surfaces were more selective towards C$_{2+}$ products than the (111) surfaces.[104–107] Based on density functional theory establishing that the energetics of the initial C–C coupling step, namely *CO–*CO coupling, were more favorable on Cu(100) relative to Cu(111), K. Jiang and collaborators used a metal ion cycling method to generate polycrystalline Cu nanocubes on Cu foil, which selectively exposed (100) facets.[108] This catalyst led to the much higher formation of C$_{2+}$ products compared to Cu(111) on polycrystalline pristine Cu foil, *i.e.*, a 6-fold increase in the C$_{2+}$ to C$_1$ product ratio when CO$_2$R was conducted in an H-cell using 0.25 M KHCO$_3$ as the electrolyte. Although ethylene was the major C$_{2+}$ product (FE = 32%), 1-propanol reached an FE of 15% at a potential of −0.963 V *vs.* RHE (partial current density 9.3 mA cm^{-2}).

Although CuS is a good catalyst for CO$_2$R to C$_1$ products, notably HCOOH and CH$_4$, a recent study showed that the introduction of double sulfur vacancies, generated by an electrochemical lithium tuning strategy (CuS + Li$^+$ + e$^-$ → CuS$_x$ + Li$_2$S), led to a large FE$_{propanol}$ of up to 15.4%, using an H-cell with 0.1 M KHCO$_3$ as the electrolyte at an applied potential of −1.05 V *vs.* RHE, giving a partial current density of about 3.0 mA cm^{-2}, which was 10-times larger than that obtained with a CuS catalyst without sulfur vacancies.[109] A much lower FE$_{propanol}$ was obtained using a flow cell and 1.0 M KOH as the electrolyte. Furthermore DFT calculations showed that owing to the presence of these vacancies, both *CO and *C$_2$ (*OCCO)

Table 4 Propanol formation from CO$_2$R (using Cu-based catalysts with FE > 15%)

| Catalysts | Conditions | Partial current density | | |
		Potential *vs.* RHE	FE (%)	Ref.
Cu(100)-rich	H-cell	9.3 mA cm^{-2}	15	108
Cu nanocubes	0.25 M KHCO$_3$	−0.96 V		
CuSx-DSV	H-cell	3 mA cm^{-2}	15.4	109
	0.1 M KHCO$_3$	−1.05 V		
Hex-2Cu–O	H-cell	1.7 mA cm^{-2}	18	112
	0.1 M KHCO$_3$	−1.2 V		
CuOD–Cu	H-cell	4 mA cm^{-2}	17.9	94
	0.1 M KHCO$_3$	−0.94 V		
R–Cu–C	H-cell	8.2 mA cm^{-2}	17.3	113
	0.1 M KHCO$_3$	−1.05 V		
Cu$_2$O–Cu	H-cell	6.8 mA cm^{-2}	16.2	114
	0.1 M KHCO$_3$	−1.4 V		
Au$_{0.02}$Cu$_{0.98}$-NR (Au-doped Cu nanorods)	Flow cell	12.6 mA cm^{-2}	18	117
	1.0 M KOH	−0.41 V		
Cu$_{94}$Ag$_6$ alloy^a	H-cell (CO$_2$ supersaturated)	12 mA cm^{-2}	39.6 (2-Propanol)	118
	1 M CsHCO$_3$	−0.73 V		
	P = 1 bar	59 mA cm^{-2}	56.7 (2-Propanol)	
	P = 10 bar	−0.7 V		

^{a} In all other cases, the product is 1-propanol, and the Cu$_{94}$Ag$_6$ alloy produces only 2-propanol.
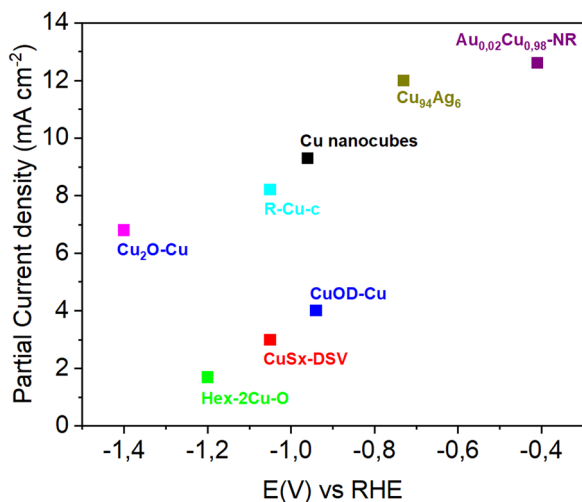
Fig. 4 Catalysts for CO_2R to propanol in H-cells; partial current density as a function of applied cathode cell voltage. Data are given in Table 4.

intermediates were stabilized and the *CO–OCCO* coupling was favored.[109]

It has been discovered that Cu-phtalocyanines and N,Cu-doped carbon materials, containing single Cu sites consisting of Cu^{2+} ions in N-coordination, are precursors of the small Cu clusters transiently formed during CO_2R, as shown by *operando* characterization techniques. It has been well established that the formation of C_2 products, notably ethanol, is due to the activity of these clusters in both cases.[110,111] This led B. Yang and coworkers to explore a series of molecular dinuclear Cu^{2+} complexes using N-based macrocyclic ligands, including expanded porphyrins such as hexaphyrins and octaphyrins.[112] In one case, a high $Fe_{propanol}$ of 18% (together with $FE_{ethanol}$ of 32%) was obtained at an applied potential of -1.2 V *vs.* RHE (total current density of 9.4 mA cm^{-2}) using an H-cell with the complex loaded onto a Ketjen black cathode and 0.1 M CO_2-saturated $KHCO_3$ as the electrolyte. Post-electrolysis characterization by mass spectrometry, UV-visible spectroscopy, X-ray photoelectron spectroscopy (XPS), microscopy and X-ray absorption spectroscopy (XAS) consistently showed that the complex was partially reduced and Cu ions partly converted into small Cu^0 clusters, leading to the formation of inorganic/organic hybrids. Although the production of multi-carbon products was possible owing to C–C coupling reactions at the surface of the under-coordinated Cu clusters, as confirmed computationally, it was experimentally well established that the presence of both the partially reduced molecular complex and metallic clusters was necessary for the cathode to be selective for alcohols. However, the same catalyst tested in a flow cell using 1.0 M KOH as the electrolyte gave very low yields of propanol ($FE_{propanol} < 10\%$).

A high $FE_{propanol}$ of 17.9% was obtained using oxide-derived copper.[94] In this interesting study, metallic Cu derived from CuO (CuOD–Cu) was compared to metallic Cu derived from Cu_2O (Cu_2OD–Cu). The two materials proved distinct in terms of both structure and activity. Upon reduction under CO_2R

conditions, all the Cu ions converted rapidly into metallic Cu^0 in both cases, as shown by XAS. However, CuOD–Cu had a richer population of undercoordinated Cu sites and a rougher surface, with a higher surface Cu atom density. Furthermore, *in situ* surface-enhanced Raman measurements clearly showed that CuOD–Cu was much better at promoting the generation of surface-adsorbed *CO and *(H)OCCOH, a key C_2 intermediate, likely favoring C–C_2 coupling and the formation of C_3 products. Although both catalytic materials resulted in relatively high yields of H_2 ($FE_{H_2} > 40\%$), CO_2R carried out in an H-cell using 0.1 M $KHCO_3$ as the electrolyte led to the much higher production of propanol in the case of CuOD–Cu ($FE_{propanol} = 17.9\%$ at -0.94 V *vs.* RHE and a partial current density of 4.0 mA cm^{-2}).

Manipulating the oxidation states to combine Cu^+ and Cu^0 sites seems to favor *CO to *OCCO coupling and propanol formation. The first example concerns an R–Cu–C material, a composite of CuCl and CuO, in which the Cl^- anions serve to stabilize the Cu^+ species during electrocatalysis due to their strong affinity for Cu surfaces.[113] Actually, during electroreduction at large cathodic potentials, Cu^+ and Cu^0 coexist on the surface, as shown by XPS, (X-ray diffraction) XRD and XAS. Furthermore, the presence of abundant defect sites, favoring multi-carbon product formation, was shown from low coordination numbers. In an H-cell, this material efficiently in catalyzed the formation of alcohols. The maximum $FE_{propanol}$ of 17.3% was obtained at an applied potential of -1.05 V *vs.* RHE (with a partial current density of 8.2 mA cm^{-2}), together with an $FE_{ethanol}$ of 32.5%. A slightly lower $FE_{propanol}$ of 14% was obtained when CO_2R was carried out in a flow cell using 1 M KOH as the electrolyte at an applied potential of -1 V *vs.* RHE (270 mA cm^{-2}). In 2024, the same strategy was explored with the synthesis of a Cu-based material possessing a bicontinuous structure, assembling ultra small domains of Cu_2O and Cu, with numerous grain boundaries between the Cu_2O and Cu phases and a high roughness factor.[114] For unknown reasons, Cu_2O resisted electroreduction and the valence state of Cu fluctuated between 0.42 and 0.55 during 100 min electrolysis. Using an H-cell and 0.1 M $KHCO_3$ electrolyte, the maximum $FE_{propanol}$ of 16.2% was obtained at -1.4 V *vs.* RHE (6.8 mA cm^{-2} partial current density). A slightly lower $FE_{propanol}$ of 12.1% was obtained in a flow cell with 1 M KOH as the electrolyte and an applied current density of 0.84 A cm^{-2} (thus a partial current density of 101.6 mA cm^{-2}). *In situ* Raman spectroscopy, *in situ* attenuated total reflection surface enhanced infrared absorption spectroscopy (ATR-SEIRAS), differential electrochemical mass spectrometry (DEMS) and DFT calculations supported the mechanism of propanol formation *via* *CO–*OCCO coupling, followed by propionaldehyde formation, and then reduction to propanol.

As discussed below, high FEs for propanol were obtained during COR with bimetallic catalysts, specifically Ag- or Au-doped Cu. Recently, this has been observed in very few cases during CO_2R as well. Generally, bimetallic systems have been developed based on the working hypothesis that a tandem catalysis mechanism operates, in which Ag or Au, catalyzing

CO_2 to COR, contributes increased surface CO coverage, followed by CO spillover from Ag or Au onto Cu favoring C–C coupling.[115] The addition of foreign heavy metals can modulate the atomic ensembles for adsorbate binding and induce lattice strain and charge transfer, altogether playing a role in enhancing catalytic activity and selectivity.[116] Specifically, DFT calculations of CO_2R on Ag- or Au-doped Cu nicely showed that doping decreased the activation energy barriers for the model reactions used as indicators for C–C and C–C_2 coupling reactions, producing C_3 compounds.[85,88,117] Finally, it was shown that doping Cu with Ag or Au increased the carbophobicity of the catalyst surface, an effect disfavoring surface C-bonded reaction intermediates in the ethylene pathway, explaining why the formation of oxygenates is promoted.[51]

A record, while still limited, $FE_{propanol}$ of 18% was obtained during CO_2R with colloidal Au-doped Cu nanorods (NRs), $Au_{0.02}Cu_{0.98}$-NR, using a flow cell and 1 M KOH as the electrolyte at an applied current of 70 mA cm^{-2}, corresponding to a moderate cathodic potential of -0.41 V vs. RHE, given that larger current densities gave lower FEs.[117] This performance could be related to the increased capacity of the catalyst to maintain high CO coverage, favoring the formation of C_3 products during CO_2R, as shown by Raman studies monitoring the *CO-characteristic peaks. Furthermore, DFT calculations showed that Au doping lowers the energy barriers for *CO coupling to two *C_2 intermediates, namely *HCCH and *HCCH$_3$. These intermediates were chosen based on a previous DFT study showing that *CO–*HCCH coupling displayed the smallest kinetic barrier, among many other scenarios involving other *C_2 intermediates.[83]

Finally, a recent study showed an interesting effect of CO_2 pressure on the formation of propanol.[118] There are only a few examples of CO_2R investigations at elevated pressure,[119–123] but none before the case described here showed the formation of high amounts of C_{3+} products, although increased surface CO coverage, which can be potentially obtained by increasing the CO_2 pressure, was shown to increase C_3 product formation, including propanol.[124] The catalyst, developed by D. Voiry et al. was a dendritic $Cu_{94}Ag_6$ alloy with highly dispersed Ag atoms and preferential CuAg(100) facets on its surface, which was obtained via co-electrodeposition under conditions that prevented galvanic replacement.[118] They used a supersaturation strategy to prepare a 1 M CsHCO$_3$ electrolyte containing dissolved CO_2 at a concentration above the saturation limit via several steps of bubbling the solution with CO_2 at a pressure of 10 bar. This led to the maximum content of 0.3 M CO_2 in the supersaturated electrolyte at atmospheric pressure compared to 0.05 M by simply bubbling CO_2 at 1 bar. Using an H-cell functioning at atmospheric pressure, it led to the remarkable and intriguing formation of 2-propanol with a record FE of 39.6% at an applied potential of -0.73 V vs. RHE (partial current density 12 mA cm^{-2}). Interestingly, no C_3 product could be detected using an H-cell and electrolyte CO_2-saturated at 1 bar or using a flow cell or MEA electrolyzer, confirming the importance of elevated CO_2 concentration for the formation of 2-propanol. A Cs-based electrolyte was also required. The

selectivity increased further with an FE for 2-propanol of 56.7% at a specific current density of 59 mA cm^{-2} when the H-cell was functioning with a supersaturated solution and a CO_2 pressure of 10 bar, a system proven to be stable for 200 h operation. Thus, the data established that the high FE for 2-propanol was derived from the combination of a supersaturated electrolyte, which favored CO coverage and C–C coupling reactions, and the presence of Ag, favoring the formation of isopropanol.

Operando Raman spectroscopy showed an increased CO coverage upon CO_2 supersaturation, with an increased ratio between *CO_{bridge} (defect-like) and *CO_{atop} (terrace-like) sites. Operando FTIR also showed an increase in the *CO and *OCH_2CH_3 signals, in parallel to an increase in $FE_{isopropanol}$, suggesting that a high density of these two intermediates triggered the formation of 2-propanol under CO_2 supersaturation conditions. Finally, DFT calculations of the energies of the pathways derived from coupling the *OCH_2CH_3 intermediate to *CO showed that the selective formation of 2-propanol in the case of the CuAg alloy was due to the effect of adjacent Ag on increasing the C–O bond dissociation energy of the *$O–CH_2CH_3$ intermediate, resulting in the selective formation of 2-propanol.

Fig. 4, showing the partial current density as a function of applied potential derived from the data in Table 4, nicely shows that the doping strategy, specifically with Ag-doped Cu materials, currently offers the best impact with respect to the formation of propanol.

2.2.2. Propanol formation from COR (Table 5 and Fig. 5). Thus far, COR is the more efficient method for producing propanol with significant FEs compared to CO_2R.[28] COR is motivated by the availability of CO feedstock from industrial steel manufacturing and potentially via CO_2R to CO as well as

Table 5 Propanol formation from COR (with FE > 20%)

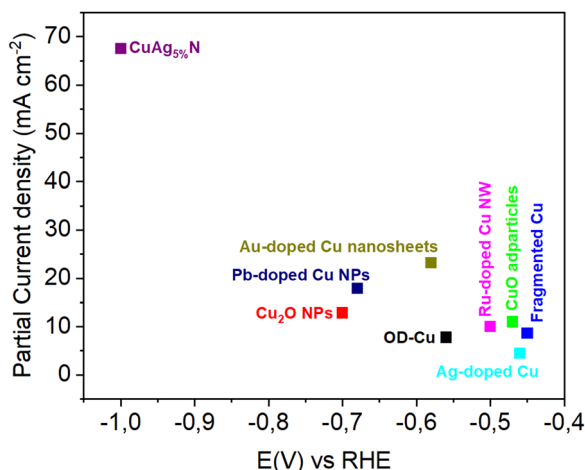| Catalysts | Conditions | Partial current density | | |
		Potential vs. RHE	FE (%)	Ref.
OD–Cu nanocavities	Flow cell 1.0 M KOH	7.77 mA cm^{-2} -0.56 V	21	124
Cu$_2$O NPs (multi hollow)	Flow cell 1.0 M KOH	12.84 mA cm^{-2} -0.7 V	30.2	127
CuO adparticles	Flow cell 1.0 M KOH	11 mA cm^{-2} -0.47 V	23	89
Fragmented Cu	Flow cell 1.0 M KOH	8.6 mA cm^{-2} -0.45 V	20	128
Ag-doped Cu	Flow cell 1.0 M KOH	4.5 mA cm^{-2} -0.46 V	33	85
AgRu-doped Cu	MEA 1.0 M KOH	111 mA cm^{-2}	37	86
Ru-doped Cu NW	Flow cell 1.0 M KOH	10 mA cm^{-2} -0.5 V	35.9	129
CuAg$_{5\%}$N	Flow cell 1.0 M CsOH	67.5 mA cm^{-2} -1 V	45	88
Au-doped Cu nanosheets	Flow cell 1.0 M KOH	23.3 mA cm^{-2} -0.58 V	46.6	95
Pb-doped Cu NPs	Flow cell 1.0 M KOH	17.86 mA cm^{-2} -0.68 V	47	90
SnCu	MEA 3.0 M KOH	70.5 mA cm^{-2}	47	130

Fig. 5 Catalysts for COR to propanol in flow cells; partial current density as a function of applied cathode cell voltage. Data are given in Table 5.

by the potential to produce compounds with longer chains. In addition, it has been shown based on technoeconomic analysis that the two-step pathway combining CO_2-to-CO and CO-to-C_{2+} electrosynthesis outperforms the one-step CO_2-to-C_{2+} electroconversion in terms of selectivity and energy efficiency, as mentioned above.[125] Commercial Cu nanoparticles and almost any Cu-based catalysts produce propanol with $FE_{propanol}$ of about 10–15% during COR in flow cells operating at applied current densities of $-100/-300$ mA cm^{-2}.[28] In one case, using the standard Cu_2O precatalyst, an FE of 22% was obtained at a very low potential (-0.44 V vs. RHE; total current density of 26 mA cm^{-2}).[126] Here, we discuss only catalysts providing FE > 20% (Table 5).

Various strategies have been explored to stabilize and concentrate *C_2 intermediates, favoring coupling to *CO or other *C_1 adsorbed species and the formation of C_3 compounds. However, in general, high selectivity for propanol is achieved at a low overpotential, and thus at a low current density. The first example involved the introduction of OD–Cu via the gentle acidic etching of Cu_2O in nanocavities, allowing a confinement effect.[124] In this case, using a flow cell with 1 M KOH electrolyte, a peak $FE_{propanol}$ of 21% was obtained at -0.56 V vs. RHE (total current density of 37 mA cm^{-2}), with decreased values at more cathodic potentials and larger current densities. This catalyst was unstable, undergoing reconstruction into aggregates during electrolysis, and thus becoming much less selective for propanol. In 2022, this strategy was further developed.[127] Multi-hollow Cu_2O nanoparticles containing nanocavities were synthesized via the reduction of copper acetate with hydrazine hydrate, followed by etching with HCl, and tested for COR in a flow cell using 1 M KOH as the electrolyte. The maximum $FE_{propanol}$ of 30.2% was obtained at an applied current density of 42.5 mA cm^{-2}. Based on this interesting finding, G. Wu and collaborators used a two-step tandem catalytic system (consisting of a first flow electrolyzer converting CO_2 selectively into CO and a second flow cell using multi-hollow Cu_2O nanoparticles at the cathode for electrolyzing the CO gas derived from the former) and achieved propanol formation from CO_2 with an FE of 15.9%.[125]

The second example involved the introduction of adparticles, which are small clusters with a size of a few nm and possess a high population of low-coordinated sites, on the surface of metallic Cu.[89] Adparticle growth on Cu could be achieved via the electroreduction of a Cu oxide precursor under a flow of CO. This rough surface was expected to increase the CO coverage and stabilize the *C_2 intermediates, and DFT calculations established that it also allows lower energy barriers for *CO–*C_2 (specifically *OCCOH and *CCH$_2$ intermediates) coupling. Actually, this catalyst deposited on a GDL resulted in a peak $FE_{propanol}$ of 23% at -0.47 V vs. RHE (partial current density of 11 mA cm^{-2}), using a flow cell and 1 M KOH as the electrolyte. The role of adparticles in this selectivity was confirmed by the significant decrease in $FE_{propanol}$ upon erasing the adparticle texture via thermal-annealing under N_2 gas. The third example involved using fragmented Cu, exhibiting a high degree of distinct facet fragments, based on the fact that the *C_1 intermediates are preferentially stabilized on Cu(111), while the *C_2 intermediates are stabilized on Cu(100).[131,132] Based on a Cu surface model with interfaces between the Cu(100) and Cu(111) domains, DFT calculations showed that this combination lowers the barriers of both *CO–*CO and *CO–*OCCO coupling reactions.[128] This fragmented catalyst, with a large density of fragments of Cu(100) and Cu(111) that are adjacent to each other, and thus with an abundance of sites, where the two facets conjoin, could be obtained via CuO synthesis from cuprous iodide, a salt allowing slow nucleation and the generation of a variety of crystalline phases. Employing this catalyst in a flow cell and using 1 M KOH as the electrolyte, CuO was reduced to metallic Cu and an $FE_{propanol}$ of 20% was obtained at -0.45 V vs. RHE (with a total current density of 43 mA cm^{-2}).[128] Less fragmented control samples, with less interfaces between the two types of facets, were less selective for propanol. Finally, it was shown that increasing the catalyst loading on a GDL potentially provides a way to stabilize and accumulate the *C_2 intermediates before they diffuse out as C_2 products, favoring their coupling to *CO and the formation of C_3 products.[133] Using commercial Cu nanoparticles, propanol production increased dramatically upon increasing the catalyst loading during COR in a flow cell with 1 M KOH electrolyte from 2% at 1.0 mg cm^{-2} to 20% at 10 mg cm^{-2} (partial current density 31 mA cm^{-2} at 4.0 V cell potential). A simulation confirmed an increase in the *C_2 intermediate retention time in the catalyst layer as a function of catalyst loading.

Another recently developed strategy favoring C_3 product formation from COR, specifically propanol, is doping Cu-based materials with one or two heavy metals. There are several examples of bi- and tri-metallic M- and M,M′-doped Cu catalysts reported in the literature exhibiting quite high $FE_{propanol}$. The stimulation of C_3 product formation was ascribed to various effects of doping with main group metals possessing a large radius, such as Ag, Au and Pb. Due to the larger radius of these metals compared to that of Cu, doping may produce surface compressive strain and increase the number of low-

coordinated sites within a defect-rich Cu structure.[85,134] These sites are known to favour *CO surface coverage, and thus *CO–*CO and *CO–*C$_2$ coupling.[89,93,96] It was shown by DFT calculations that the diversity of Cu atoms environments is responsible for the asymmetric C–C coupling active sites, which decrease the energy barriers for *CO dimerization and the *CO–*OCCO coupling reaction.[85] The calculations were performed for a series of dopants, Pd, Ru, Rh, Ag and Au, among which the largest effects on the reaction barriers were obtained for Ag doping. Other computational studies, based on a larger scope of the most stable computed C$_2$ intermediates on Cu (100), confirmed that the presence of Ag or Au atoms on Cu results in a large decrease in the activation barriers of *C$_2$–*CO coupling reactions.[88,95] Furthermore, CuAg materials are prone to favor alcohols vs. hydrocarbons, which can be rationalized through the principle of lowering the *C affinity, given that Ag addition renders the surface more carbophobic.[51]

The first reported example of an Ag-doped Cu (atomic Ag percentage of 4%) COR catalyst, prepared by the galvanic exchange reaction between Cu nanoparticles and silver nitrate, allowed the formation of propanol with high selectivity (FE = 33%, partial current density of 4.5 mA cm^{-2}) at −0.46 V vs. RHE in a flow cell reactor with 1 M KOH electrolyte.[85] The selectivity decreased upon applying a more cathodic potential, indicating that C–C$_2$ coupling becomes slower at high potential, favoring C$_2$ protonation and the formation of C$_2$ products such as ethylene. Later, the same authors slightly increased the FE$_{propanol}$ to 37% using an Ru/Ag-doped Cu material, which was prepared via a two-step galvanic exchange between Cu and RuCl$_3$, followed by AgNO$_3$.[86] This performance was obtained with an MEA electrolyzer using 1 M KOH as the anolyte, with an applied current density of 300 mA cm^{-2} associated with a full cell voltage of 2.75 V. Interestingly, this selectivity was maintained during long-term electrolysis (100 h). This result was supported by DFT calculations, showing that the addition of Ru to Ag-doped Cu was the most effective dopant in decreasing the energy barriers of *CO dimerization and *CO coupling to *OCCO compared to Au, Pd, Ni, Fe and Pt.

Following the same strategy, more recently, Ru–CuNW, CuO-derived Cu^0 nanowires doped with Ru (1 at%) without Ru phase segregation, showed high selectivity for propanol with an FE of 35.9% at −0.5 V vs. RHE from COR (corresponding to a low partial density of about 10 mA cm^{-2}) using a flow cell and 1 M KOH as the electrolyte.[129] This selectivity was proposed notably by DFT calculations to derive from the combination of a low-coordinated Cu step surface favoring alcohol formation vs. ethylene,[97] as shown by XAS analysis on the Cu edge of the activated catalyst, with the presence of a doped heavy metal displaying high CO affinity, thus favoring *C$_2$ intermediate coupling to *CO for propanol formation. This agreed with the much lower FE for propanol with the undoped CuNW catalyst (FE = 22%). However, electrolysis at a more cathodic potential and higher current densities led to a decrease in the FE for propanol.

Although metal doping was mainly achieved on Cu NPs or OD–Cu (oxide-derived Cu), a recent study showed that silver or gold doping on copper nitride, Cu$_3$N, resulted in significantly higher selectivity in COR for propanol.[88] The CuAg$_{5\%}$N catalyst, consisting of Cu$_3$N nanoparticles and nanorods doped with metallic Ag, was prepared via a galvanic replacement reaction using CuNPs and AgNO$_3$, followed by calcination, and then a nitridation step, consisting of pyrolysis in the presence of NaNH$_2$. Subsequently, it was used at the cathode of a flow cell using 1 M CsOH as the electrolyte, allowing COR reduction with a remarkable FE$_{propanol}$ of 45% at a high applied current density of 150 mA cm^{-2} (−1 V vs. RHE), which was found to be stable over 9 h electrolysis. In situ XAS and XRD showed that under catalytic conditions, Cu$_3$N was totally reduced to metallic Cu^0, indicating that the catalytic species are nitride-derived copper (ND–Cu) sites. Although the pristine Cu NPs, OD–Cu and ND–Cu all possessed catalytic Cu^0 sites, intriguingly ND–Cu was different from that derived from the two other materials, given that different product distributions in COR were obtained. Thus, further investigation is needed to better understand the specific local structure, surface coordination and electronic properties of the ND–Cu sites that make them unique in favoring propanol formation.

Gold is indeed another metal used for doping Cu. A recent study reported the propanol-selective activity of a Cu material doped with Au NPs.[95] Au NPs (6.1 wt%) were homogeneously deposited on the surface of CuO nanosheets before electroreduction under CO. This led to the reconstruction of the material, during which Cu species migrated to the surface of Au NPs, leading to a disordered layer of Cu atoms around Au NPs. The detailed EXAFS analysis indicated a lower Cu–Cu coordination number on RCu/Au (R for reconstructed) compared to the control undoped RCu sample, indicating that Au doping is responsible for the presence of rich undercoordinated sites. Employing this catalyst and a flow cell with 1 M KOH as the electrolyte, an FE$_{propanol}$ of 46.6% was obtained at −0.58 V vs. RHE with a total current density of 50 mA cm^{-2}. The FE dropped to 25% at more cathodic potentials; however, leading to a partial current density for propanol formation at −0.78 V vs. RHE of 124 mA cm^{-2}.

Finally, Pb-doped Cu NPs, obtained by the electrodeposition of Pb atoms onto oxide-derived Cu surfaces in the presence of CO, proved to be excellent catalysts for COR to propanol.[90] SEM and TEM analysis showed that Pb deposition led to the formation of small grains and a surface rich in grain boundaries (GB), which are not observed on the control undoped Cu catalyst. A higher density of Pb atoms was present in the GB zones, suggesting that the Pb doping is the origin of the formation of GBs and the increased density of undercoordinated Cu sites, as confirmed by XAS. Furthermore, operando Raman spectroscopy measurements during COR showed stronger *CO binding on the Pb–Cu sample compared to the undoped Cu. Employing this Pb–Cu material, containing 8% Pb atoms, and using a flow cell and 1 M KOH electrolyte, a record FE$_{propanol}$ of 47% was obtained at −0.68 V vs. RHE (current density 38 mA cm^{-2}), while the highest value was 28% at a more cathodic potential in the case of the undoped OD–Cu. Variations in the Pb loading and CO partial pressure,

Table 6 Butanol formation from CO_2R (Cu catalysts)

Catalysts	Conditions	Partial current density		Products	FE (%)	Ref.
		Potential vs. RHE				
OD–Cu	Flow cell 1.0 M KOH	0.08 mA cm^{-2} −0.48 V		1-Butanol	0.056%	72
CuP$_2$	Flow cell 0.5 M KHCO$_3$	<0.12 mA cm^{-2} −0.6 V		1-Butanol	3.9%	137
CuTi	H-cell 0.1 M KHCO$_3$	2 mA cm^{-2} −0.8 V		1-Butanol (+acetone)	6.85% (11.14%)	138
Cu-Ir	H-cell 0.1 M KHCO$_3$	0.21 mA cm^{-2} −0.57 V		*Tert*-Butanol (+acetone)	14.8% (5.0%)	139

as well as *operando* ATR-SEIRAS, clearly indicated that the improvement in propanol formation was well related to Pb favoring CO binding and enhancing the *CO coverage, thus favoring C–C coupling up to C$_3$ products. A stable FE$_{propanol}$ of 30% (current density of 76 mA cm^{-2}) was obtained using an MEA electrolyzer during 110 h electrolysis.

During the revision of this article, an interesting study was reported, showing that metallic Cu doped with dispersed Sn atoms (Sn–Cu) was highly selective for propanol formation during COR using an MEA electrolyzer and 3.0 M KOH electrolyte (Table 5).[130] An FE$_{propanol}$ of 47% was obtained at an applied current density of 150 mA cm^{-2} and the system was proven to be stable for 120 h. This was consistent with DFT calculations establishing that the combination of Cu with Sn atoms favors C1–C2 coupling better than other combinations (Zn–Cu, Ga–Cu, In–Cu, Sb–Cu, Pb–Cu and Bi–Cu). Furthermore, owing to the construction of an Sn–Cu/carbon/ionomer heterojunction, propanol crossover through the membrane was greatly limited, achieving a high concentration of propanol (30 wt%) at the cathode after 120 h electrolysis, a concentration that minimizes the downstream separation cost.

Fig. 5 summarizes the best catalysts and partial current density for propanol from COR in flow cells as a function of applied potential, illustrating the superiority of metal-doped Cu materials, as is the case for CO$_2$R to propanol (Fig. 4).

2.2.3. Acetone formation from CO$_2$R. Here, it is necessary to discuss a report describing the catalytic activity of N-doped and Cu-doped porous carbon (CuNC), containing isolated Cu sites, in which the Cu ions are coordinated by a combination of pyrrolic and pyridinic N atoms. CO$_2$R, conducted in an H-cell with a 0.1 M KHCO$_3$ CO$_2$-saturated electrolyte, gave, in addition to CO and HCOOH, large amounts of C$_{2+}$ products, *i.e.*, acetic acid, ethanol and even acetone.[135] A record FE for acetone of 36.7% was obtained at an applied potential of −0.36 V vs. RHE, and thus at a low current density (5 mA cm^{-2}). DFT calculations showed that C–C coupling could occur on the surfaces containing only isolated Cu sites. This result is intriguing for the following reasons. Firstly, comparable CuNC catalysts led to the formation of ethanol but not acetone.[111] Secondly, as discussed above, the active species during CuNC-dependent CO$_2$R were found to be Cu clusters, transiently and reversibly formed during catalysis, and not the isolated sites, as unambiguously demonstrated by *operando* characterization

techniques.[111,136] In the report discussed here, only *ex situ* characterization techniques were used, raising doubts regarding the involvement of single sites as the catalytic species. Considering the importance of generating acetone selectively from CO$_2$R, this system should be further investigated.

2.2.4. Butanol formation *via* CO$_2$R (Table 6). Owing to the utilization of a GDE in a flow cell, alkaline electrolyte (1 M KOH) and highly sensitive analytical methods, the presence of butanol, together with the major C$_2$ products (ethylene, ethanol) and propanol (FE = 6.5%), could be observed for the first time during CO$_2$R using CuO-derived Cu as the catalyst.[72] Although the production was limited, with an FE of 0.056% and a partial current density j_{BuOH} of −0.08 mA cm^{-2} at a low applied potential of −0.48 V vs. RHE (lower FEs were obtained at more cathodic potentials), attempts have been made to understand the mechanism for butanol formation. Based on experimental and theoretical studies, the standard mechanism implying C–C coupling of four individual C$_1$ adsorbed intermediates, such as *CO, has been excluded. Instead it has been proposed that the reaction proceeds *via* a combination of electrochemical and thermal steps, as shown in Fig. 6. After the electroreduction of CO$_2$ to acetaldehyde, crotonaldehyde is formed *via* the aldol condensation of two molecules of acetaldehyde, promoted by HO$^-$, and its electroreduction first generates butanal, and then butanol. This agrees with the detection of small amounts of acetaldehyde and crotonaldehyde. This mechanism was supported by control electrolysis experiments. For example, the electroreduction of 50 mM acetaldehyde under the same conditions indeed generated 1-butanol (FE = 9.6%), together with ethanol as the major product. Also, 1-butanol was formed during the electroreduction of crotonaldehyde and butanal, with FE = 14.8% and FE = 17.3%, respectively, the complement being H$_2$. The FEs for butanol were even larger (FE = 46%) when electrolysis was carried out at neutral pH, indicating that aldehydes are more reactive than their geminal diols, which likely form under alkaline conditions. Since then, there has been no report on CO$_2$R producing butanol with higher FEs using pure Cu. This limitation is likely due to the fact that Cu materials show little activity for acetaldehyde production, and furthermore very high activity for the electroreduction of acetaldehyde into ethanol. Although Fe, among several metals, shows the highest FEs for butanol during the electrolysis of acetaldehyde and
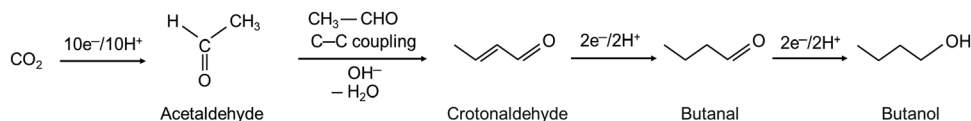
Fig. 6 Proposed mechanism for butanol formation.[72]

crotonaldehyde, unfortunately it is inefficient in promoting C–C coupling from CO_2.[72]

However, recently, butanol formation was reported to be increased using copper phosphide, CuP_2, as the catalyst.[137] Using a flow cell with a 9.0 cm^{-2} electrode and 0.5 M $KHCO_3$ as the electrolyte, the maximum FE of 3.9% was obtained at a very low applied potential of −0.6 V vs. RHE (resulting in a very low current density of <3.0 mA cm^{-2}). XPS and HAADF-STEM-EDS (high-angle annular dark field scanning transmission electron microscopy energy-dispersive X-ray spectroscopy) indicated that copper phosphide was partially covered with phosphate and that phosphorous was partially leached, forming copper oxide after CO_2R. Although no mechanistic studies were carried out, a mechanism was proposed for butanol production, which was very similar to that proposed for Ni- and Fe-phosphide-based CO_2R to C_3 and C_4 products (Fig. 1). In contrast to the usual Cu-based catalysts, the vibrational bands associated with adsorbed *CO could not be observed, thus excluding the involvement of CO–CO coupling during the formation of butanol. CuP_2, with highly oxophilic surfaces due to the presence of P atoms, is likely to favor the conversion of CO_2 to formate rather than CO as the first reaction step. The reduction of formate to formaldehyde and condensation of two molecules of formaldehyde, followed by water elimination, can generate acetaldehyde. Then, the reaction proceeds via the mechanism shown in Fig. 6, i.e., the aldol condensation of two molecules of acetaldehyde, generating crotonaldehyde, which is finally reduced to butanol. Accordingly, the electroreduction of formate under identical conditions was shown to produce acetaldehyde, while the electroreduction of acetaldehyde produced 1-butanol.

Following these studies, several reports showed the potential of bimetallic M–Cu materials to catalyze the electroreduction of CO_2R to butanol with larger FEs (Table 6). The first one described an amorphous CuTi alloy, in which Ti is expected to transfer electrons to and increase the electron density of the coordinatively unsaturated Cu active sites.[138] Given that Ti is prone to favor HER over CO_2R, the surface Ti is further dealloyed in a dilute HF solution, forming the a-CuTi@Cu catalyst. Employing this catalyst, the highest FE value for

butanol (FE = 6.85%) was obtained in an H-cell with 0.1 M $KHCO_3$ as the electrolyte at an applied potential of −0.8 V vs. RHE, the major products being H_2 and ethanol (FE = 24%), together with a C_3 product, namely acetone (FE = 11,14%) and small amounts of C_1 products (mainly methanol). Although DFT calculations showed that subsurface Ti atoms favored C–C coupling on the Cu active sites, no insight was presenting into why this catalyst allowed the relatively high formation of a C_4 compound.

The second study used a $Cu_{0.48}Ir_{0.52}$ alloy, Cu–Ir, as shown in Table 6.[139] This catalyst, in an H-cell with 0.1 M $KHCO_3$ electrolyte mainly generated H_2 (FE = 67%), together with C_1 products (methanol and formic acid accounting for FE = 14%), but most remarkably acetone and tert-butanol. Under the optimized applied potential of 0.57 V vs. RHE, with a total current density of −1.4 mA cm^{-2}, tert-butanol was obtained with an FE of 14.8%, a current record, and acetone with FE = 5%. The formation of acetone and tert-butanol requires 16- and 24-electron transfer, respectively. It was proposed that acetone is an intermediate towards tert-butanol via CO insertion into adsorbed acetone, given that the addition of acetone to the electrolyte during electrolysis increased the production of tert-butanol. DFT calculations showed that this reaction is thermodynamically favorable. Thus, the reaction was proposed to proceed via *CO–*CO coupling, followed by a series of proton-coupled electron transfers, generating the CH_3CH_2O* intermediate. The presence of an oxophilic metal (Ir) favors binding of the intermediates via the O atom and stabilizes the C–O bond. The oxygen atom is retained during CO insertion and further reduction leads to adsorbed acetone. At this stage, either acetone is released in solution or it further reacts with a fourth molecule of CO to generate tert-butanol after the elimination of water and reduction (see Fig. 7).

2.3. C_{3+} hydrocarbon formation via CO_2R (Table 7)

Propylene is an important chemical feedstock, in particular for the polymer industry, reaching an annual global capacity of about 150 Mt; however, with a parallel emission of about 100 Mt of CO_2, given that its current production is entirely derived from crude oil. Propane is used as a fuel source for
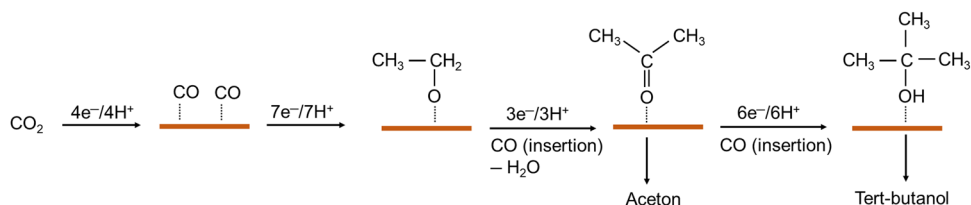

Fig. 7 Proposed mechanism for the formation of tert-butanol catalyzed by $Cu_{0.48}Ir_{0.52}$ alloy.[139]

Table 7 C_{3+} hydrocarbons from CO_2R (Cu catalysts)

Catalysts	Conditions	Applied total current Potential vs. RHE	Products	FE (%)	Ref.
Cu nanocubes	MEA	200 mA cm^{-2}	Propylene	<1	140
Cu$_2$O–Cu	H-cell	7 mA cm^{-2}	Propanol	8.7	71
			Propane	0.9	
	0.1 M KCl	−1.6 V	Propylene	1	
			Butane	0.9	
CuNanoCs	Flow cell	0.6 A cm^{-2}	Propanol	4	144
	1.0 M KOH	−0.6 V	Propylene	1.4	
	0.2 M CsI		Allyl alcohol	0.5	
Bi–Cu$_2$O nanowire	Filter-press cell	45 mA cm^{-2}	Propane	85	145
	0.1 M KHCO$_3$				
Cu$_2$O/Ti$_3$C$_2$T$_x$MXene	H-cell	35 mA cm^{-2}	Propane	3.3	146
	0.1 M KHCO$_3$	−1.3 V			

ovens and furnaces in the production of glass, ceramics, and other materials as well as for boilers in the manufacturing of paper products, textiles, and plastics. CO_2RR and COR using renewable electricity may be an interesting alternative for the production of these C_3 hydrocarbons. However, propylene and propane are rarely observed during CO_2R and COR using Cu-based catalysts. Here, we describe the most important systems showing this capability.

Using Cu nanocubes and an MEA-type electrolyzer, CO_2R at an applied current density of 200 mA cm^{-2} resulted in the production of H_2 and ethylene as the major products together with very small amounts of propylene ($j_{C_3H_4}$ = 1.5 mA cm^{-2} and FE < 1%).[140]

Using a biphasic Cu$_2$O–Cu catalyst and KCl electrolyte during 1 h electrolysis in an H-cell, in addition to the usual C_2 products ethylene and ethanol (total FE 45%), not only a relatively high FE of 8.7% for propanol was obtained but also low amounts of propane and propylene (FE = 1%), and for the first time, butane, a C_4 product, with a FE of 0.9%.[71] However, during longer electrolysis, productivity of the catalyst towards C_3–C_4 products declined with time. This was correlated with the decline in the surface Cu$^+$/Cu^0 ratio, as shown by XPS analysis and *operando* Cu K-edge XANES, suggesting the importance of the Cu$^+$ sites for promoting the formation of hydrocarbons with long chains. Furthermore, it was shown that the KCl electrolyte played a critical role in slowing down the reduction of the oxide to the metallic phase. It was proposed that Cl adsorption stabilized the Cu$_2$O phase, allowing higher binding energy for CO adsorption and increasing the CO coverage, which is known to favor C–C coupling reactions. The stronger CO adsorption on a surface containing Cu$^+$ sites has been studied theoretically and experimentally, as well as the increase in CO binding due to the presence of ad-atoms such as Cl.[141–143]

More recently, the significant production of ethylene was reported during CO_2R using Cu nanocrystals (CuNanoCs) as catalysts and an alkaline flow cell.[144] The surface of CuNanoCs predominantly consisted of Cu(100) and Cu(111) facets, with a distribution that remained unchanged during long-term electrolysis, despite the considerable reconstruction of their morphology. As mentioned earlier, the presence of both types of facets is an interesting property given that Cu(100) was shown

to favour the propagation of carbon chains,[74] while its coexistence with Cu(111) provides sites stabilizing the key intermediates for multi-carbon products.[128] CO_2R at −0.6 V vs. RHE led to the formation of ethylene (FE = 50%) and ethanol (FE = 15%) as the major CO_2-derived products, together with propanol (FE = 4%) and propylene accounting for an FE of 1.4%. A partial current density of 5.5 mA cm^{-2} was obtained at a slightly lower applied potential (−0.65 V vs. RHE). Surprisingly, only trace amounts of propylene (FE = 0.06%) could be detected during COR under similar electrolysis conditions, while ethylene was still produced with a high FE. This led to the intriguing consideration that propylene was unlikely to be derived from surface *CO coupling to *C$_2$ intermediates and that the active *C$_1$ intermediate was missing in CO electrolysis. This led to the hypothesis that the key *C$_1$ intermediate involved in the propylene pathway was either adsorbed CO_2 or *COOH. This is in contrast with the propanol pathway in which the C_3 backbone is formed via *CO–*C$_2$ coupling,[84] in agreement with the observation that the formation of propanol was less affected by the change in the feed gas. The working mechanistic hypothesis for propylene formation was nicely substantiated by isotopic labeling experiments using various mixtures of $^{12}CO_2/^{13}CO_2$ and $^{12}CO/^{13}CO$. Notably, using the $^{13}CO_2/^{12}CO$ = 20%/80% mixture, the majority of the formed ethylene had two ^{12}C atoms, while the majority of formed propylene had two ^{12}C atoms and one ^{13}C atom, in agreement with the hypothesis that propylene arises from the coupling of $^{13}CO_2$ or *$^{13}COOH$ intermediates with the *C$_2$ species that are produced from ^{12}COR and are precursors of ethylene (and ethanol). The reason why the *C$_3$ intermediate, derived from the coupling of three *CO molecules, involved in the propanol pathway does not produce propylene may be kinetic. Interestingly, the same study evaluated a broad library of monometallic, bimetallic and trimetallic Cu-based catalysts (a total of 20 different materials) and none gave FE larger than 1.8% for propylene formation.[128]

An interesting report showed that bismuth-doped copper nanowires were active for the formation of propane.[145] Cu foam was converted into Cu nanowires (NWs), on which Bi was electrodeposited using different deposition times. Characterization of the material showed that the Cu foam was covered

with Cu_2O NWs and Bi particles. Using a filter-press cell working at constant current density of -45 mA cm^{-2} with 0.1 M KHCO$_3$ or 0.45 M KHCO$_3$ + 0.5 M KCl as the catholyte, different products were obtained. In the second case, the major product was formate (FE = 86%) and HER (FE$_{H_2}$ = 10%) was limited. In the first case, HER increased slightly and formate decreased to 5–30%, depending on the Bi electrodeposition time. However, the most interesting and intriguing observation was the production of a C$_3$ hydrocarbon, specifically propane, with very high selectivity, where the highest amount (FE = 85%) was obtained with the sample derived from the longest Bi electrodeposition time. This gave a record partial current density for propane of 38 mA cm^{-2}. Unfortunately, the origin of this selectivity was not studied, and thus this material clearly deserves further investigation.

Finally, propane has also been observed during CO$_2$R with a substantial FE of 3.3% using a Cu$_2$O/MXene catalyst, in which Cu$_2$O nanoparticles were deposited on titanium carbide (Ti$_3$C$_2$T$_x$), a 2D material known as MXene.[146] These results were obtained using an H-cell with a CO$_2$-saturated 0.1 M KHCO$_3$ catholyte, at a cathodic potential of -1.3 V vs. RHE (current density of about 35 mA cm^{-2}). A much lower FE of 0.1% was obtained using the Cu/MXene catalyst, whereas no propane could be detected using Cu-free MXene. In all cases, the major products were CO and H$_2$. The importance of combining Cu$_2$O and MXene for propane formation was rationalized by DFT calculations, where Cu$_2$O and MXene stabilize the *C$_2$ and *CO intermediates, respectively, thus favoring *C$_2$–*CO coupling at the interface of the two components.

3. Conclusion

The deep analysis of the current knowledge regarding CO$_2$R and COR to C$_{3+}$ compounds provided in this review leads to the following notable observations and perspectives.

(1) Further investigation of the potential of CO$_2$R/COR to generate C$_{3+}$ products

Indeed, it is possible to generate a variety of C$_{3+}$ compounds via CO$_2$R and COR, with quite high selectivity, the most common being propanol (Tables 4 and 5). For example, C$_4$ molecules such as butanol, methylglyoxal and furandiol are sometimes formed with reasonable selectivity (Tables 3 and 6). Although rare, C$_5$ and C$_6$ compounds have also been observed; however, with very low current densities and faradaic efficiencies. Except in a few cases, as discussed below, oxygenated compounds (alcohols and acetone) are generally more abundant than hydrocarbons, although the remarkable formation of propane, with quite high faradaic efficiency, has been reported; however, without being reproduced in the literature thus far (Tables 3 and 7).[38,145]

These results are summarized in Table 2, showing the most industrially relevant C$_3$ and C$_4$ products and highlighting the potential of CO$_2$R and COR for alcohols and alkanes synthesis. Presently, alcohols are important commodity chemicals.

Beyond their current uses, new high-volume applications such as precursors for the production of synthetic aviation fuels may arise in the future. Alkanes, such as propane and butane, have the highest market volume to date due to their use as fuels. However, this might be reduced in the future because of the electrification of the applications using propane and butane as fuel today. In the case of olefins, although they can be synthesized from CO$_2$R or COR derived alkanes, such as propylene from propane, via thermal dehydrogenation, direct CO$_2$R or COR to propylene would be much preferred. This will result in lower capital expenditures compared to pathways relying on CO$_2$ hydrogenation using electrolytic H$_2$. It should be noted that in some cases, small amounts of propylene were observed (Tables 3 and 7), justifying further studies aimed at improving the corresponding catalysts. Table 2 also shows that butadiene is the C$_4$ olefin with the highest market volume, larger than that of butene. However, thus far, there is no study reporting butadiene formation from CO$_2$R or COR. These considerations indicate the potential for further optimizing catalysts for C$_{3+}$ alcohols, propane and propylene formation.

(2) Re-evaluating non-Cu materials as catalysts for CO$_2$R/COR

It is timely and worth reinvestigating non-Cu metals, in particular Mo, Fe and Ni, as catalysts for these reactions. However, these metals suffer from strong limitations, the most important one being their low productivity in general. As shown in Table 1, C$_{3+}$ compounds are mostly formed at quite low overpotentials, and thus with very low current densities in most cases. Indeed, increased polarization results in the increased production of H$_2$, which is greatly favored on the surface of these metals because they are prone to adsorbing H atoms from protons and providing hydridic surfaces, where the reactivity of the latter with protons exceeds that with CO$_2$. Furthermore, they display too strong *CO binding, which favors HER.[52] Thus, efforts should be devoted to weakening the *CO adsorption energy on the surface of these non-Cu metals. One interesting illustration of the possibility to allow Fe- and Ni-based materials to efficiently catalyze CO$_2$ activation is the case of Fe- and Ni-based single-atom catalysts (SACs).[147–149] They exhibit much lower *CO binding strength compared to their bulk metal counterparts; however, too low that they can catalyze CO$_2$R to CO exclusively with almost FE$_{CO}$ = 100%, with no further conversion to C$_{2+}$ products. Further research on Fe- and Ni-based catalysts should focus on tuning their *CO binding energy to achieve mild strength comparable to that on Cu. Presently, there is no clear trend regarding the correlation between structure/morphology and selectivity/productivity with this class of catalysts, and thus no rationale pointing to obvious targets. Therefore, a large variety of potential catalysts should be explored. Whether artificial intelligence and machine learning can play a role in this respect is an open question.[150–152]

(3) Exploring surface modification of non-Cu catalysts

Mo$_3$P-Im is a unique catalyst for CO$_2$R to propane with very high selectivity (FE = 91%) and high current density (390 mA cm^{-2}).[38] It is interesting to note that this is the only example of a non-Cu

material whose activity and selectivity has been tuned by surface molecular modification, a strategy that has been largely and successfully used for improving the performances of Cu-based catalysts.[153,154] This strategy can be used more systematically in the case of non-Cu metals for improving the selectivity, in particular with modifications preventing HER, and thus allowing the higher productivity of CO_2-derived compounds at larger current densities.

(4) Gaining deeper insight into the reaction mechanisms in the case of non-Cu catalysts

Reactivity studies coupled with spectroscopic and microscopic characterization of catalysts under *in situ* and *operando* conditions and DFT calculations, in the case of simple catalysts whose modelling is accessible, and despite the multitude of possible intermediates, may give deeper insight into the mechanisms, which are still far from understood. Interestingly, the few studies available seem to suggest mechanisms significantly different from that proposed and partly established for Cu-based catalysts, thus involving different reactive intermediates such as formaldehyde and acetaldehyde in the case of Ni- and Fe-based materials.[40,46,56] Indeed, given that C–C coupling occurs at potentials excluding CO_2 activation, it is very likely, as generally proposed, that the reaction does not proceed *via* *CO–*CO coupling. Instead, it might in some cases involve formaldehyde intermediate formation, followed by a series of thermal aldehyde condensation steps, as in the case of Ni- and Fe-phosphides. Based on this, one should consider future research on engineering (multi)metallic materials that combine low kinetic barriers for CO_2R to formic acid, and then to formaldehyde with catalytic activity for thermal aldehyde self-condensation. Thus far, although Ru-, Co-, Ni- and Fe-based materials show some catalytic potential for the latter, there are exceedingly few good systems for producing formaldehyde from CO_2R or COR.[155–159]

(5) Further investigating multi-metallic Cu-based catalysts

Cu is still the metal of choice and has been extensively studied during the last 20 years. Tuning its morphology and surface as well as the reaction conditions (pressure, electrolyte, and flow rate) has recently led to improved selectivity in particular for propanol formation *via* both CO_2R and COR. Propanol is the most important C_{3+} product in Cu-based CO_2R and COR, where in the case of CO_2R, there are still very few Cu-based systems achieving $FE_{propanol}$ exceeding 15%, while the record $FE_{propanol}$ of almost 50% has been obtained *via* COR. Improvements have been obtained through strategies aimed at stabilizing the *C_2 intermediates to allow *CO–*C_2 coupling including confinement effects owing to the introduction of nanocavities, facet engineering, or tuning the catalyst layer and the CO_2 pressure. The most effective way to favor propanol formation, both in CO_2R and COR, is consistently *via* the introduction of dopants (Ag, Au, and Pb), which leads to *C_2 stabilization and favors *CO–*C_2 coupling, as supported by DFT calculations, owing to the surface compressive strain and increase in low-coordination sites and grain boundaries. These initial studies

should encourage the further extensive exploration of combinations of metal dopants on Cu-based materials towards not only bimetallic but also polymetallic materials for propanol formation *via* CO_2R and COR.

(6) Further studies on the selectivity for oxygenates/ hydrocarbons

Cu-based materials promoting the formation of C_{3+} hydrocarbons are still lacking, with only a few exceptions, such as the Bi-doped Cu catalyst described above with a unique FE value of 85% for propane.[145] Also, it is still necessary to better understand how to control the selectivity for oxygenates/hydrocarbons to favour the formation of propylene and propane, which have been observed only rarely and with low selectivity in general. The other limitation of Cu-based catalysts is the general absence of C_4 compounds, with the exception of *tert*-butanol formation *via* CO_2R, with the maximum FE of 14.8% in the case of a Cu–Ir alloy material,[139] again suggesting the prevalence of alcohols over hydrocarbons. It is very likely that this is due to the impossibility thus far to engineer Cu surfaces to stabilize the *C_3 intermediates and allow them to couple with *CO towards C_4 products before the C_3 products desorb from their surface. It should be noted that no C_{4+} products have been reported during COR.

(7) Investigating tandem pathways

Although the formation of C_{3+} compounds *via* CO_2R and COR provides an opportunity to valorize CO_2 into industrially relevant products, the scope of compounds is still limited to C_3 and C_4 derivatives. It is not unlikely that producing more complex molecules with a larger carbon number will be significantly more difficult. Indeed, an increase in the number of electrons and protons to be transferred results in lower reaction kinetics and an increased number of possible products, making it difficult to achieve high partial current densities and faradaic efficiencies for a target product, and thus limiting the industrial interest towards the direct synthetic approach. Under these conditions, CO_2-derived complex molecules should preferentially be synthesized *via* a tandem scenario, converting CO_2R/COR-derived C_2/C_3 products *via* mature and inexpensive thermochemical processes for reactions such as oligomerization and aromatization.

Data availability

No primary research results, software or code have been included, and no new data were generated or analysed as part of this review.

Conflicts of interest

There are no conflicts of interest to declare.

Acknowledgements

References

1 Y. Li, F. Zhu, E. Liu, H. Ouyang, W. Lu, H. Gu, J. Ren, W. Peng, H. Hou and Y. He, *Adv. Compos. Hybrid Mater.*, 2024, **7**, 147.

2 M. N. Anwar, A. Fayyaz, N. F. Sohail, M. F. Khokhar, M. Baqar, A. Yasar, K. Rasool, A. Nazir, M. U. F. Raja, M. Rehan, M. Aghbashlo, M. Tabatabaei and A. S. Nizami, *J. Environ. Manage.*, 2020, **260**, 110059.

3 S. C. Peter, *ACS Energy Lett.*, 2018, **3**, 1557–1561.

4 E. T. C. Vogt and B. M. Weckhuysen, *Nature*, 2024, **629**, 295–306.

5 P. De Luna, C. Hahn, D. Higgins, S. A. Jaffer, T. F. Jaramillo and E. H. Sargent, *Science*, 2019, **364**, eaav3506.

6 R. G. Grim, J. R. Ferrell Iii, Z. Huang, L. Tao and M. G. Resch, *Joule*, 2023, **7**, 1684–1699.

7 X. Tan, C. Yu, Y. Ren, S. Cui, W. Li and J. Qiu, *Energy Environ. Sci.*, 2021, **14**, 765–780.

8 S. Nitopi, E. Bertheussen, S. B. Scott, X. Liu, A. K. Engstfeld, S. Horch, B. Seger, I. E. L. Stephens, K. Chan, C. Hahn, J. K. Nørskov, T. F. Jaramillo and I. Chorkendorff, *Chem. Rev.*, 2019, **119**, 7610–7672.

9 G. Leonzio, A. Hankin and N. Shah, *Chem. Eng. Res. Des.*, 2024, **208**, 934–955.

10 W. Lai, Y. Qiao, J. Zhang, Z. Lin and H. Huang, *Energy Environ. Sci.*, 2022, **15**, 3603–3629.

11 D. Wakerley, S. Lamaison, J. Wicks, A. Clemens, J. Feaster, D. Corral, S. A. Jaffer, A. Sarkar, M. Fontecave, E. B. Duoss, S. Baker, E. H. Sargent, T. F. Jaramillo and C. Hahn, *Nat. Energy*, 2022, **7**, 130–143.

12 D. Wu, F. Jiao and Q. Lu, *ACS Catal.*, 2022, **12**, 12993–13020.

13 T. N. Nguyen and C.-T. Dinh, *Chem. Soc. Rev.*, 2020, **49**, 7488–7504.

14 J. Han, X. Bai, X. Xu, X. Bai, A. Husile, S. Zhang, L. Qi and J. Guan, *Chem. Sci.*, 2024, **15**, 7870–7907.

15 X. Zhang, S.-X. Guo, K. A. Gandionco, A. M. Bond and J. Zhang, *Mater. Today Adv.*, 2020, **7**, 100074.

16 D. Ewis, M. Arsalan, M. Khaled, D. Pant, M. M. Ba-Abbad, A. Amhamed and M. H. El-Naas, *Sep. Purif. Technol.*, 2023, **316**, 123811.

17 Z. Liu, J. Qian, G. Zhang, B. Zhang and Y. He, *Sep. Purif. Technol.*, 2024, **330**, 125177.

18 L. Fan, C. Xia, F. Yang, J. Wang, H. Wang and Y. Lu, *Sci. Adv.*, 2023, **6**, eaay3111.

19 B. Chang, H. Pang, F. Raziq, S. Wang, K.-W. Huang, J. Ye and H. Zhang, *Energy Environ. Sci.*, 2023, **16**, 4714–4758.

20 Y. Y. Birdja, E. Pérez-Gallent, M. C. Figueiredo, A. J. Göttle, F. Calle-Vallejo and M. T. M. Koper, *Nat. Energy*, 2019, **4**, 732–745.

21 B. Li, L. Liu, M. Yue, Q. Niu, M. Li, T. Zhang, W. Xie and Q. Wang, *Green Chem.*, 2024, **26**, 103–121.

22 Z. Sun, Y. Hu, D. Zhou, M. Sun, S. Wang and W. Chen, *ACS Energy Lett.*, 2021, **6**, 3992–4022.

23 Y. Yan, L. Ke, Y. Ding, Y. Zhang, K. Rui, H. Lin and J. Zhu, *Mater. Chem. Front.*, 2021, **5**, 2668–2683.

24 L. Xie, Y. Jiang, W. Zhu, S. Ding, Y. Zhou and J.-J. Zhu, *Chem. Sci.*, 2023, **14**, 13629–13660.

25 J. A. Rabinowitz and M. W. Kanan, *Nat. Commun.*, 2020, **11**, 5231.

26 C. Chen, Y. Li and P. Yang, *Joule*, 2021, **5**, 737–742.

27 A. Ozden, Y. Wang, F. Li, M. Luo, J. Sisler, A. Thevenon, A. Rosas-Hernández, T. Burdyny, Y. Lum, H. Yadegari, T. Agapie, J. C. Peters, E. H. Sargent and D. Sinton, *Joule*, 2021, **5**, 706–719.

28 N. S. Romero Cuellar, K. Wiesner-Fleischer, M. Fleischer, A. Rucki and O. Hinrichsen, *Electrochim. Acta*, 2019, **307**, 164–175.

29 M. Jouny, G. S. Hutchings and F. Jiao, *Nat. Catal.*, 2019, **2**, 1062–1070.

30 Y. Ji, A. Guan and G. Zheng, *Cell Rep. Phys. Sci.*, 2022, **3**, 101072.

31 J. Sisler, S. Khan, A. H. Ip, M. W. Schreiber, S. A. Jaffer, E. R. Bobicki, C.-T. Dinh and E. H. Sargent, *ACS Energy Lett.*, 2021, **6**, 997–1002.

32 A. Perazio, C. E. Creissen, J. G. Rivera de la Cruz, M. W. Schreiber and M. Fontecave, *ACS Energy Lett.*, 2023, **8**, 2979–2985.

33 J. E. Huang, F. Li, A. Ozden, A. Sedighian Rasouli, F. P. García de Arquer, S. Liu, S. Zhang, M. Luo, X. Wang, Y. Lum, Y. Xu, K. Bertens, R. K. Miao, C.-T. Dinh, D. Sinton and E. H. Sargent, *Science*, 2021, **372**, 1074–1078.

34 X. Zhong, H.-J. Peng, C. Xia and X. Liu, *J. Mater. Chem. A*, 2024, **12**, 19663–19684.

35 S. J. Raaijman, M. P. Schellekens, P. J. Corbett and M. T. M. Koper, *Angew. Chem., Int. Ed.*, 2021, **60**, 21732–21736.

36 R. Kortlever, I. Peters, C. Balemans, R. Kas, Y. Kwon, G. Mul and M. T. M. Koper, *Chem. Commun.*, 2016, **52**, 10229–10232.

37 S. A. Francis, J. M. Velazquez, I. M. Ferrer, D. A. Torelli, D. Guevarra, M. T. McDowell, K. Sun, X. Zhou, F. H. Saadi, J. John, M. H. Richter, F. P. Hyler, K. M. Papadantonakis, B. S. Brunschwig and N. S. Lewis, *Chem. Mater.*, 2018, **30**, 4902–4908.

38 M. Esmaeilirad, Z. Jiang, A. M. Harzandi, A. Kondori, M. Tamadoni Saray, C. U. Segre, R. Shahbazian-Yassar, A. M. Rappe and M. Asadi, *Catalysts*, 2021, **11**, 330.

39 A. R. Paris and A. B. Bocarsly, *ACS Catal.*, 2017, **7**, 6815–6820.

40 K. U. D. Calvinho, A. B. Laursen, K. M. K. Yap, T. A. Goetjen, S. Hwang, N. Murali, B. Mejia-Sosa, A. Lubarski, K. M. Teeluck, E. S. Hall, E. Garfunkel, M. Greenblatt and G. C. Dismukes, *Energy Environ. Sci.*, 2018, **11**, 2550–2559.

41 M. Dhiman, Y. Chen, Y. Li, A. B. Laursen, K. U. D. Calvinho, T. G. Deutsch and G. C. Dismukes, *J. Mater. Chem. A*, 2023, **11**, 717–725.

42 M.-G. Kim, Y. Choi, E. Park, C.-H. Cheon, N.-K. Kim, B. K. Min and W. Kim, *ACS Appl. Energy Mater.*, 2020, **3**, 11516–11522.

43 Y. Zhou, A. J. Martín, F. Dattila, S. Xi, N. López, J. Pérez-Ramírez and B. S. Yeo, *Nat. Catal.*, 2022, **5**, 545–554.

44 S. P. Cronin, S. Dulovic, J. A. Lawrence, K. A. Filsinger, A. P. Hernandez-Gonzalez, R. Evans, J. W. Stiles, J. Morris, I. Pelczer and A. B. Bocarsly, *J. Am. Chem. Soc.*, 2023, **145**, 6762–6772.

45 Y. J. Kim, J. Y. Maeng, S. Y. Hwang, J. H. Yang, I. Yoon, C. W. Myung, C. K. Rhee and Y. Sohn, *Nano Energy*, 2023, **118**, 108995.

46 K. U. D. Calvinho, A. W. Alherz, K. M. K. Yap, A. B. Laursen, S. Hwang, Z. J. L. Bare, Z. Clifford, C. B. Musgrave and G. C. Dismukes, *J. Am. Chem. Soc.*, 2021, **143**, 21275–21285.

47 P. Preikschas, J. Zhang, R. R. Seemakurthi, Z. Lian, A. J. Martín, S. Xi, F. Krumeich, H. Ma, Y. Zhou, N. López, B. S. Yeo and J. Pérez-Ramírez, *Adv. Energy Mater.*, 2024, **14**, 2401447.

48 H. Mahmoudi, M. Mahmoudi, O. Doustdar, H. Jahangiri, A. Tsolakis, S. Gu and M. LechWyszynski, *Biofuels Eng.*, 2017, **2**, 11–31.

49 Z. Teimouri, N. Abatzoglou and A. K. Dalai, 2021, **11**.

50 X. Zhang, S. Hua, L. Lai, Z. Wang, T. Liao, L. He, H. Tang and X. Wan, *RSC Adv.*, 2022, **12**, 17959–17983.

51 H.-J. Peng, M. T. Tang, J. Halldin Stenlid, X. Liu and F. Abild-Pedersen, *Nat. Commun.*, 2022, **13**, 1399.

52 Y. Hori, H. Wakebe, T. Tsukamoto and O. Koga, *Electrochim. Acta*, 1994, **39**, 1833–1839.

53 F. Studt, I. Sharafutdinov, F. Abild-Pedersen, C. F. Elkjær, J. S. Hummelshøj, S. Dahl, I. Chorkendorff and J. K. Nørskov, *Nat. Chem.*, 2014, **6**, 320–324.

54 D. A. Torelli, S. A. Francis, J. C. Crompton, A. Javier, J. R. Thompson, B. S. Brunschwig, M. P. Soriaga and N. S. Lewis, *ACS Catal.*, 2016, **6**, 2100–2104.

55 P. Bui, J. A. Cecilia, S. T. Oyama, A. Takagaki, A. Infantes-Molina, H. Zhao, D. Li, E. Rodríguez-Castellón and A. Jiménez López, *J. Catal.*, 2012, **294**, 184–198.

56 S. Banerjee, A. Kakekhani, R. B. Wexler and A. M. Rappe, *ACS Catal.*, 2021, **11**, 11706–11715.

57 R. E. Vos and M. T. M. Koper, *ACS Catal.*, 2024, **14**, 4432–4440.

58 J. Y. Maeng, S. Y. Hwang, Y. J. Kim, I. Yoon, C. W. Myung, C. K. Rhee and Y. Sohn, *J. Phys. Chem. C*, 2023, **127**, 11448–11461.

59 J. Y. Maeng, S. Y. Hwang, C. K. Rhee and Y. Sohn, *Appl. Surf. Sci.*, 2023, **631**, 157576.

60 X. Liu, Y. Hou, F. Yang, Y. Liu, H. Yu, X. Han, J. Chen, S. Chen, S. Zhou, S. Deng and J. Wang, *Carbon*, 2023, **201**, 460–466.

61 L. Ji, L. Li, X. Ji, Y. Zhang, S. Mou, T. Wu, Q. Liu, B. Li, X. Zhu, Y. Luo, X. Shi, A. M. Asiri and X. Sun, *Angew. Chem., Int. Ed.*, 2020, **59**, 758–762.

62 L. Ji, L. Chang, Y. Zhang, S. Mou, T. Wang, Y. Luo, Z. Wang and X. Sun, *ACS Catal.*, 2019, **9**, 9721–9725.

63 P. Chen, P. Zhang, X. Kang, L. Zheng, G. Mo, R. Wu, J. Tai and B. Han, *J. Am. Chem. Soc.*, 2022, **144**, 14769–14777.

64 S. Hanselman, M. T. M. Koper and F. Calle-Vallejo, *ACS Energy Lett.*, 2018, **3**, 1062–1067.

65 Y. Ji, X. Lv, R. Wei, A. Guan, C. Yang, Y. Yan, M. Kuang and G. Zheng, *Angew. Chem., Int. Ed.*, 2024, **63**, e202411194.

66 W. Zhang, J. Ai, T. Ouyang, L. Yu, A. Liu, L. Han, Y. Duan, C. Tian, C. Chu, Y. Ma, S. Che and Y. Fang, *J. Am. Chem. Soc.*, 2024, **146**, 28214–28221.

67 D. W. Stephan, *Science*, 2016, **354**, aaf7229.

68 H.-T. Kim, J. Park, J. Mun, H. Shin, D.-H. Roh, J. Kwon, S. Kim, S.-J. Kim, G. Lee, S. J. Kang and T.-H. Kwon, *ACS Catal.*, 2024, **14**, 10392–10402.

69 K. P. Kuhl, E. R. Cave, D. N. Abram and T. F. Jaramillo, *Energy Environ. Sci.*, 2012, **5**, 7050–7059.

70 A. H. M. da Silva, G. Karaiskakis, R. E. Vos and M. T. M. Koper, *J. Am. Chem. Soc.*, 2023, **145**, 15343–15352.

71 S. Lee, D. Kim and J. Lee, *Angew. Chem., Int. Ed.*, 2015, **54**, 14701–14705.

72 L. R. L. Ting, R. García-Muelas, A. J. Martín, F. L. P. Veenstra, S. T.-J. Chen, Y. Peng, E. Y. X. Per, S. Pablo-García, N. López, J. Pérez-Ramírez and B. S. Yeo, *Angew. Chem., Int. Ed.*, 2020, **59**, 21072–21079.

73 A. J. Garza, A. T. Bell and M. Head-Gordon, *ACS Catal.*, 2018, **8**, 1490–1499.

74 F. Calle-Vallejo and M. T. M. Koper, *Angew. Chem., Int. Ed.*, 2013, **52**, 7282–7285.

75 H. Peng, M. T. Tang, X. Liu, P. Schlexer Lamoureux, M. Bajdich and F. Abild-Pedersen, *Energy Environ. Sci.*, 2021, **14**, 473–482.

76 R. Kortlever, J. Shen, K. J. P. Schouten, F. Calle-Vallejo and M. T. M. Koper, *J. Phys. Chem. Lett.*, 2015, **6**, 4073–4082.

77 T. K. Todorova, M. W. Schreiber and M. Fontecave, *ACS Catal.*, 2020, **10**, 1754–1768.

78 I. V. Chernyshova, P. Somasundaran and S. Ponnurangam, *Proc. Natl. Acad. Sci. U. S. A.*, 2018, **115**, E9261–E9270.

79 S. Jiang, K. Klingan, C. Pasquini and H. Dau, *J. Chem. Phys.*, 2018, **150**, 041718.

80 X. Li, S. Wang, L. Li, Y. Sun and Y. Xie, *J. Am. Chem. Soc.*, 2020, **142**, 9567–9581.

81 C. Zhan, F. Dattila, C. Rettenmaier, A. Herzog, M. Herran, T. Wagner, F. Scholten, A. Bergmann, N. López and B. Roldan Cuenya, *Nat. Energy*, 2024, **9**, 1485–1496.

82 J. Santatiwongchai, K. Faungnawakij and P. Hirunsit, *ACS Catal.*, 2021, **11**, 9688–9701.

83 M. T. Tang, H.-J. Peng, J. H. Stenlid and F. Abild-Pedersen, *J. Phys. Chem. C*, 2021, **125**, 26437–26447.

84 S. Pablo-García, F. L. P. Veenstra, L. R. L. Ting, R. García-Muelas, F. Dattila, A. J. Martín, B. S. Yeo, J. Pérez-Ramírez and N. López, *Catal. Sci. Technol.*, 2022, **12**, 409–417.

85 X. Wang, Z. Wang, T.-T. Zhuang, C.-T. Dinh, J. Li, D.-H. Nam, F. Li, C.-W. Huang, C.-S. Tan, Z. Chen, M. Chi, C. M. Gabardo, A. Seifitokaldani, P. Todorović, A. Proppe, Y. Pang, A. R. Kirmani, Y. Wang, A. H. Ip, L. J. Richter, B. Scheffel, A. Xu, S.-C. Lo, S. O. Kelley, D. Sinton and E. H. Sargent, *Nat. Commun.*, 2019, **10**, 5186.

86 X. Wang, P. Ou, A. Ozden, S.-F. Hung, J. Tam, C. M. Gabardo, J. Y. Howe, J. Sisler, K. Bertens, F. P. García de Arquer, R. K. Miao, C. P. O'Brien, Z. Wang, J. Abed, A. S. Rasouli, M. Sun, A. H. Ip, D. Sinton and E. H. Sargent, *Nat. Energy*, 2022, **7**, 170–176.

87 X. Chang, A. Malkani, X. Yang and B. Xu, *J. Am. Chem. Soc.*, 2020, **142**, 2975–2983.

88 H. Phong Duong, J. G. Rivera de la Cruz, N.-H. Tran, J. Louis, S. Zanna, D. Portehault, A. Zitolo, M. Walls, D. V. Peron, M. W. Schreiber, N. Menguy and M. Fontecave, *Angew. Chem., Int. Ed.*, 2023, **62**, e202310788.

89 J. Li, F. Che, Y. Pang, C. Zou, J. Y. Howe, T. Burdyny, J. P. Edwards, Y. Wang, F. Li, Z. Wang, P. De Luna, C.-T. Dinh, T.-T. Zhuang, M. I. Saidaminov, S. Cheng, T. Wu, Y. Z. Finfrock, L. Ma, S.-H. Hsieh, Y.-S. Liu, G. A. Botton, W.-F. Pong, X. Du, J. Guo, T.-K. Sham, E. H. Sargent and D. Sinton, *Nat. Commun.*, 2018, **9**, 4614.

90 W. Niu, Z. Chen, W. Guo, W. Mao, Y. Liu, Y. Guo, J. Chen, R. Huang, L. Kang, Y. Ma, Q. Yan, J. Ye, C. Cui, L. Zhang, P. Wang, X. Xu and B. Zhang, *Nat. Commun.*, 2023, **14**, 4882.

91 H. Li, P. Wei, T. Liu, M. Li, C. Wang, R. Li, J. Ye, Z.-Y. Zhou, S.-G. Sun, Q. Fu, D. Gao, G. Wang and X. Bao, *Nat. Commun.*, 2024, **15**, 4603.

92 X. K. Lu, B. Lu, H. Li, K. Lim and L. C. Seitz, *ACS Catal.*, 2022, **12**, 6663–6671.

93 K. Jiang, Y. Huang, G. Zeng, F. M. Toma, W. A. Goddard, III and A. T. Bell, *ACS Energy Lett.*, 2020, **5**, 1206–1214.

94 C. Long, X. Liu, K. Wan, Y. Jiang, P. An, C. Yang, G. Wu, W. Wang, J. Guo, L. Li, K. Pang, Q. Li, C. Cui, S. Liu, T. Tan and Z. Tang, *Sci. Adv.*, 2023, **9**, eadi6119.

95 C. Long, K. Wan, Y. Chen, L. Li, Y. Jiang, C. Yang, Q. Wu, G. Wu, P. Xu, J. Li, X. Shi, Z. Tang and C. Cui, *J. Am. Chem. Soc.*, 2024, **146**, 4632–4641.

96 T. Cheng, H. Xiao and W. A. Goddard, *J. Am. Chem. Soc.*, 2017, **139**, 11642–11645.

97 Z. Gu, H. Shen, Z. Chen, Y. Yang, C. Yang, Y. Ji, Y. Wang, C. Zhu, J. Liu, J. Li, T.-K. Sham, X. Xu and G. Zheng, *Joule*, 2021, **5**, 429–440.

98 C. W. Li, J. Ciston and M. W. Kanan, *Nature*, 2014, **508**, 504–507.

99 D. Ren, N. T. Wong, A. D. Handoko, Y. Huang and B. S. Yeo, *J. Phys. Chem. Lett.*, 2016, **7**, 20–24.

100 A. Verdaguer-Casadevall, C. W. Li, T. P. Johansson, S. B. Scott, J. T. McKeown, M. Kumar, I. E. L. Stephens, M. W. Kanan and I. Chorkendorff, *J. Am. Chem. Soc.*, 2015, **137**, 9808–9811.

101 D. Zhong, Z.-J. Zhao, Q. Zhao, D. Cheng, B. Liu, G. Zhang, W. Deng, H. Dong, L. Zhang, J. Li, J. Li and J. Gong, *Angew. Chem., Int. Ed.*, 2021, **60**, 4879–4885.

102 Y. Hori, I. Takahashi, O. Koga and N. Hoshi, *J. Mol. Catal. A: Chem.*, 2003, **199**, 39–47.

103 A. H. M. da Silva, Q. Lenne, R. E. Vos and M. T. M. Koper, *ACS Catal.*, 2023, **13**, 4339–4347.

104 Y. Huang, A. D. Handoko, P. Hirunsit and B. S. Yeo, *ACS Catal.*, 2017, **7**, 1749–1756.

105 K. J. P. Schouten, Z. Qin, E. Pérez Gallent and M. T. M. Koper, *J. Am. Chem. Soc.*, 2012, **134**, 9864–9867.

106 Y. Hori, I. Takahashi, O. Koga and N. Hoshi, *J. Phys. Chem. B*, 2002, **106**, 15–17.

107 F. S. Roberts, K. P. Kuhl and A. Nilsson, *Angew. Chem., Int. Ed.*, 2015, **54**, 5179–5182.

108 K. Jiang, R. B. Sandberg, A. J. Akey, X. Liu, D. C. Bell, J. K. Nørskov, K. Chan and H. Wang, *Nat. Catal.*, 2018, **1**, 111–119.

109 C. Peng, G. Luo, J. Zhang, M. Chen, Z. Wang, T.-K. Sham, L. Zhang, Y. Li and G. Zheng, *Nat. Commun.*, 2021, **12**, 1580.

110 Z. Weng, Y. Wu, M. Wang, J. Jiang, K. Yang, S. Huo, X.-F. Wang, Q. Ma, G. W. Brudvig, V. S. Batista, Y. Liang, Z. Feng and H. Wang, *Nat. Commun.*, 2018, **9**, 415.

111 D. Karapinar, N. T. Huan, N. Ranjbar Sahraie, J. Li, D. Wakerley, N. Touati, S. Zanna, D. Taverna, L. H. Galvão Tizei, A. Zitolo, F. Jaouen, V. Mougel and M. Fontecave, *Angew. Chem., Int. Ed.*, 2019, **58**, 15098–15103.

112 B. Yang, L. Chen, S. Xue, H. Sun, K. Feng, Y. Chen, X. Zhang, L. Xiao, Y. Qin, J. Zhong, Z. Deng, Y. Jiao and Y. Peng, *Nat. Commun.*, 2022, **13**, 5122.

113 D. Tan, B. Wulan, J. Ma, X. Cao and J. Zhang, *Chem. Catal.*, 2023, **3**, 100512.

114 R. Zhang, J. Zhang, S. Wang, Z. Tan, Y. Yang, Y. Song, M. Li, Y. Zhao, H. Wang, B. Han and R. Duan, *Angew. Chem., Int. Ed.*, 2024, **63**, e202405733.

115 C. G. Morales-Guio, E. R. Cave, S. A. Nitopi, J. T. Feaster, L. Wang, K. P. Kuhl, A. Jackson, N. C. Johnson, D. N. Abram, T. Hatsukade, C. Hahn and T. F. Jaramillo, *Nat. Catal.*, 2018, **1**, 764–771.

116 J. D. Lee, J. B. Miller, A. V. Shneidman, L. Sun, J. F. Weaver, J. Aizenberg, J. Biener, J. A. Boscoboinik, A. C. Foucher, A. I. Frenkel, J. E. S. van der Hoeven, B. Kozinsky, N. Marcella, M. M. Montemore, H. T. Ngan, C. R. O'Connor, C. J. Owen, D. J. Stacchiola, E. A. Stach, R. J. Madix, P. Sautet and C. M. Friend, *Chem. Rev.*, 2022, **122**, 8758–8808.

117 S. Jeong, C. Huang, Z. Levell, R. X. Skalla, W. Hong, N. J. Escorcia, Y. Losovyj, B. Zhu, A. N. Butrum-Griffith, Y. Liu, C. W. Li, D. Reifsnyder Hickey, Y. Liu and X. Ye, *J. Am. Chem. Soc.*, 2024, **146**, 4508–4520.

118 K. Qi, Y. Zhang, N. Onofrio, E. Petit, X. Cui, J. Ma, J. Fan, H. Wu, W. Wang, J. Li, J. Liu, Y. Zhang, Y. Wang, G. Jia, J. Wu, L. Lajaunie, C. Salameh and D. Voiry, *Nat. Catal.*, 2023, **6**, 319–331.

119 M. Ramdin, A. R. T. Morrison, M. de Groen, R. van Haperen, R. de Kler, L. J. P. van den Broeke, J. P. M. Trusler, W. de Jong and T. J. H. Vlugt, *Ind. Eng. Chem. Res.*, 2019, **58**, 1834–1847.

120 C. I. Shaughnessy, D. J. Sconyers, T. A. Kerr, H.-J. Lee, B. Subramaniam, K. C. Leonard and J. D. Blakemore, *ChemSusChem*, 2019, **12**, 3761–3768.

121 C. M. Gabardo, A. Seifitokaldani, J. P. Edwards, C.-T. Dinh, T. Burdyny, M. G. Kibria, C. P. O'Brien, E. H. Sargent and D. Sinton, *Energy Environ. Sci.*, 2018, **11**, 2531–2539.

122 J. P. Edwards, Y. Xu, C. M. Gabardo, C.-T. Dinh, J. Li, Z. Qi, A. Ozden, E. H. Sargent and D. Sinton, *Appl. Energy*, 2020, **261**, 114305.

123 S. Lamaison, D. Wakerley, J. Blanchard, D. Montero, G. Rousse, D. Mercier, P. Marcus, D. Taverna, D. Giaume, V. Mougel and M. Fontecave, *Joule*, 2020, **4**, 395–406.

124 T.-T. Zhuang, Y. Pang, Z.-Q. Liang, Z. Wang, Y. Li, C.-S. Tan, J. Li, C. T. Dinh, P. De Luna, P.-L. Hsieh, T. Burdyny, H.-H. Li, M. Liu, Y. Wang, F. Li, A. Proppe, A. Johnston, D.-H. Nam, Z.-Y. Wu, Y.-R. Zheng, A. H. Ip, H. Tan, L.-J. Chen, S.-H. Yu, S. O. Kelley, D. Sinton and E. H. Sargent, *Nat. Catal.*, 2018, **1**, 946–951.

125 J. M. Spurgeon and B. Kumar, *Energy Environ. Sci.*, 2018, **11**, 1536–1551.

126 J. Li, Z. Wang, C. McCallum, Y. Xu, F. Li, Y. Wang, C. M. Gabardo, C.-T. Dinh, T.-T. Zhuang, L. Wang, J. Y. Howe, Y. Ren, E. H. Sargent and D. Sinton, *Nat. Catal.*, 2019, **2**, 1124–1131.

127 G. Wu, Y. Song, Q. Zheng, C. Long, T. Fan, Z. Yang, X. Huang, Q. Li, Y. Sun, L. Zuo, S. Lei and Z. Tang, *Adv. Energy Mater.*, 2022, **12**, 2202054.

128 Y. Pang, J. Li, Z. Wang, C.-S. Tan, P.-L. Hsieh, T.-T. Zhuang, Z.-Q. Liang, C. Zou, X. Wang, P. De Luna, J. P. Edwards, Y. Xu, F. Li, C.-T. Dinh, M. Zhong, Y. Lou, D. Wu, L.-J. Chen, E. H. Sargent and D. Sinton, *Nat. Catal.*, 2019, **2**, 251–258.

129 G. Zhou, B. Li, G. Cheng, C. J. Breckner, D. P. Dean, M. Yang, N. Yao, J. T. Miller, J. B. M. Klok, N. Tsesmetzis, G. Wang and Z. J. Ren, *J. Am. Chem. Soc.*, 2024, **146**, 31788–31798.

130 Y. Chen, X. Wang, X.-Y. Li, R. K. Miao, J. Dong, Z. Zhao, C. Liu, J. E. Huang, J. Wu, S. Chu, W. Ni, Z. Guo, Y. Xu, P. Ou, B. Xu, Y. Hou, D. Sinton and E. H. Sargent, *Nat. Catal.*, 2025, **8**, 239–247.

131 H. Xiao, T. Cheng and W. A. Goddard, III, *J. Am. Chem. Soc.*, 2017, **139**, 130–136.

132 A. Loiudice, P. Lobaccaro, E. A. Kamali, T. Thao, B. H. Huang, J. W. Ager and R. Buonsanti, *Angew. Chem., Int. Ed.*, 2016, **55**, 5789–5792.

133 S. Guo, Y. Liu, Y. Huang, H. Wang, E. Murphy, L. Delafontaine, J. L. Chen, I. V. Zenyuk and P. Atanassov, *ACS Energy Lett.*, 2023, **8**, 935–942.

134 H. Xiao, W. A. Goddard, T. Cheng and Y. Liu, *Proc. Natl. Acad. Sci. U. S. A.*, 2017, **114**, 6685–6688.

135 K. Zhao, X. Nie, H. Wang, S. Chen, X. Quan, H. Yu, W. Choi, G. Zhang, B. Kim and J. G. Chen, *Nat. Commun.*, 2020, **11**, 2455.

136 C. E. Creissen and M. Fontecave, *Nat. Commun.*, 2022, **13**, 2280.

137 M. Choi, S. Bong, J. W. Kim and J. Lee, *ACS Energy Lett.*, 2021, **6**, 2090–2095.

138 F. Hu, L. Yang, Y. Jiang, C. Duan, X. Wang, L. Zeng, X. Lv, D. Duan, Q. Liu, T. Kong, J. Jiang, R. Long and Y. Xiong, *Angew. Chem., Int. Ed.*, 2021, **60**, 26122–26127.

139 M.-G. Kim, J. Park, Y. Choi, H. C. Song, S.-H. Kim, K.-M. Bang, H. C. Ham, N.-K. Kim, D. H. Won, B. K. Min, S. J. Yoo and W. Kim, *Adv. Energy Mater.*, 2023, **13**, 2300749.

140 G. O. Larrazábal, V. Okatenko, I. Chorkendorff, R. Buonsanti and B. Seger, *ACS Appl. Mater. Interfaces*, 2022, **14**, 7779–7787.

141 D. F. Cox and K. H. Schulz, *Surf. Sci.*, 1991, **249**, 138–148.

142 L.-Y. Gan and Y.-J. Zhao, *J. Chem. Phys.*, 2010, **133**, 094703.

143 Y. Hori, A. Murata and R. Takahashi, *J. Chem. Soc., Faraday Trans. 1*, 1989, **85**, 2309–2326.

144 J. Gao, A. Bahmanpour, O. Kröcher, S. M. Zakeeruddin, D. Ren and M. Grätzel, *Nat. Chem.*, 2023, **15**, 705–713.

145 C. Azenha, C. Mateos-Pedrero, M. Alvarez-Guerra, A. Irabien and A. Mendes, *Chem. Eng. J.*, 2022, **445**, 136575.

146 J. Y. Kim, W. T. Hong, T. K. C. Phu, S. C. Cho, B. Kim, U. Baeck, H.-S. Oh, J. H. Koh, X. Yu, C. H. Choi, J. Park, S. U. Lee, C.-H. Chung and J. K. Kim, *Adv. Sci.*, 2024, **11**, 2405154.

147 W. Huang, J. Zhu, S. Liu, W. Zhang, L. Zhou and L. Mai, *EES Catal.*, 2023, **1**, 434–458.

148 X. Yan, C. Duan, S. Yu, B. Dai, C. Sun and H. Chu, *Renewable Sustainable Energy Rev.*, 2024, **190**, 114086.

149 Q. Sun, C. Jia, Y. Zhao and C. Zhao, *Chin. J. Catal.*, 2022, **43**, 1547–1597.

150 D. H. Mok, H. Li, G. Zhang, C. Lee, K. Jiang and S. Back, *Nat. Commun.*, 2023, **14**, 7303.

151 X. Ma, Z. Li, L. E. K. Achenie and H. Xin, *J. Phys. Chem. Lett.*, 2015, **6**, 3528–3533.

152 Z. Gariepy, G. Chen, A. Xu, Z. Lu, Z. W. Chen and C. V. Singh, *Energy Adv.*, 2023, **2**, 410–419.

153 O. Christensen, S. Zhao, Z. Sun, A. Bagger, J. V. Lauritsen, S. U. Pedersen, K. Daasbjerg and J. Rossmeisl, *ACS Catal.*, 2022, **12**, 15737–15749.

154 Q. Zhu, C. J. Murphy and L. R. Baker, *J. Am. Chem. Soc.*, 2022, **144**, 2829–2840.

155 C. Dong, M. Ji, X. Yang, J. Yao and H. Chen, *Catalysts*, 2017, **7**, 5.

156 A. Singh, A. Zamader, R. Khakpour, K. Laasonen, M. Busch and M. Robert, *J. Am. Chem. Soc.*, 2024, **146**, 22129–22133.

157 S. Zhao, H.-Q. Liang, X.-M. Hu, S. Li and K. Daasbjerg, *Angew. Chem., Int. Ed.*, 2022, **61**, e202204008.

158 S. Desmons, J. Bonin, M. Robert and S. Bontemps, *Chem. Sci.*, 2024, **15**, 15023–15086.

159 L. Deng, Z. Wang, X. Jiang, J. Xu, Z. Zhou, X. Li, Z. You, M. Ding, T. Shishido, X. Liu and M. Xu, *Appl. Catal., B*, 2023, **322**, 122124.